Controls on potassium incorporation in foraminifera and other marine calcifying organisms

Romi Nambiar[a,b,*], Hagar Hauzer[c,d], William R. Gray[e], Michael J. Henehan[f], Laura Cotton[g], Jonathan Erez[c], Yair Rosenthal[h], Willem Renema[i,j], Wolfgang Müller[a,b], David Evans[a,b]

[a]Institute of Geosciences, Goethe University, Frankfurt, Altenhöferallee 1, 60438 Frankfurt am Main, Germany

[b]FIERCE, Frankfurt Isotope & Element Research Center, Goethe University, Altenhöferallee 1, 60438 Frankfurt am Main, Germany

[c]The Fredy & Nadine Herrmann Institute of Earth Sciences, the Hebrew University of Jerusalem, Israel

[d]Israel Oceanographic and Limnological Research, National Institute of Oceanography, Haifa, Israel

[e]Laboratoire des Sciences du Climat et de l'Environnement (LSCE/IPSL), Université Paris-Saclay, Gif-sur-Yvette, France

[f]Section 3.3 Earth Surface Geochemistry, Deutsches GeoForschungsZentrum GFZ, 14473, Potsdam, Germany

[g]Natural History Museum of Denmark, University of Copenhagen, Denmark

[h]Department of Marine and Coastal Sciences, Rutgers, State University of New Jersey, New Brunswick, NJ, USA

[i]Naturalis Biodiversity Center, Leiden, Netherlands

[j]University of Amsterdam, Institute for Biodiversity and Ecosystem Dynamics, Amsterdam, NL

Abstract

Seawater chemistry exerts an important control on the incorporation of trace elements into the shells of marine calcifying organisms. Variability in the major ion chemistry of seawater is also an indicator of past geological processes, and so the influence of seawater chemistry on carbonate trace element incorporation can be harnessed to determine changes in the composition of seawater through time. Here, we investigate whether key oceanographic parameters (temperature, salinity, and the carbonate system) affect the incorporation of potassium (K) into foraminiferal calcite, and explore the utility of K/Ca ratios in foraminifera as an indicator of past variability in the seawater Ca^{2+} concentration. We measured both low-Mg and high-Mg modern foraminifera, including planktonic (*Globigerinoides ruber*) and shallow-dwelling larger benthic (*Operculina ammonoides*) species, using laser-ablation sector-field inductively-coupled plasma mass spectrometry (LA-SF-ICPMS). Both species show no resolvable influence of temperature, salinity, pH, or $[CO_3^{2-}]$ on K incorporation. In order to determine the effect of the seawater Ca concentration ($[Ca^{2+}]_{sw}$) on K incorporation, we

analysed laboratory-cultured *O. ammonoides*, the close living relative of the abundant Eocene *Nummulites*, grown at four different $[Ca^{2+}]_{sw}$. We find a significant relationship between seawater and shell K/Ca, albeit with a shallower slope compared to most other trace elements which we suggest is driven by a crystal growth rate effect on K incorporation, constrained using culture experiments of *O. ammonoides* grown at different pH. If the K^+ concentration has remained relatively constant throughout the Phanerozoic Eon, our data may pave the way forward for the use of K/Ca as a direct proxy for past $[Ca^{2+}]_{sw}$ variability. Alternatively, coupling K/Ca with the Na/Ca proxy would allow more accurate reconstruction of $[Ca^{2+}]_{sw}$ or verification of whether $[K^+]_{sw}$ or $[Na^+]_{sw}$ has indeed remained within narrow bounds.

Keywords: Larger Benthic Foraminifera (LBF), culture calibration, K/Ca, Na/Ca, seawater chemistry, LA-SF-ICPMS

*Corresponding author.
Email address: Nambiar@geo.uni-frankfurt.de (R. Nambiar)

1. Introduction

Trace elements in marine carbonates are widely used for palaeoclimatic reconstruction. Foraminifera are an important archive for this purpose because of their widespread abundance and good preservation potential. However, shell precipitation from the surrounding seawater is a complex, biologically controlled process (Bentov et al., 2009; De Nooijer et al., 2009). The biogeochemical imprints of this process, termed 'vital effects', are not necessarily predictable from a simple chemical thermodynamic perspective (e.g. Erez, 2003), which means that the relationship between shell chemistry and ambient physical or chemical conditions must currently be empirically calibrated (Hauzer et al., 2018; Keul et al., 2013; Lea et al., 1999; Zhou et al., 2021). Using this approach, a wide range of chemical signatures in marine carbonates have been established as palaeo-proxies. For example, trace element ratios have been extensively applied to reconstruct parameters such as ocean temperature (Mg/Ca and Li/Mg; Rosenthal et al., 1997; Lea et al., 1999; Anand et al., 2003; Marchitto et al., 2018; Gray and Evans, 2019), the carbonate system (B/Ca, Zn/Ca; Marchitto et al., 2000; Yu et al., 2010; Brown et al., 2011; Allen and Hönisch, 2012; Van Dijk et al., 2017), salinity (Ba/Ca; Weldeab et al., 2007), nutrient concentration (Cd/Ca; Boyle, 1981; Rickaby and Elderfield, 1999). On longer (multi-million year) timescales, the application of foraminiferal trace element proxies is complicated by the fact that variability in seawater chemistry also affects the incorporation of trace elements into foraminifer's shells. For instance, variability in seawater Mg/Ca affects the Mg/Ca of foraminifera and thus complicates its use as palaeotemperature proxy (Evans and Müller, 2012; Hasiuk and Lohmann, 2010; Segev and Erez, 2006). Because ocean chemistry has undergone substantial secular changes throughout the Phanerozoic (Lowenstein et al., 2001; Turchyn and DePaolo, 2019; Wilkinson and Algeo, 1989), this issue constitutes a major source of uncertainty in the

application of element/Ca proxies in deep time. To enable the accurate application of trace element-based palaeoclimatic proxies beyond the residence time of calcium (~1 Myr; Broecker and Peng, 1982), precise and accurate reconstructions of seawater major ion chemistry are required.

Long-term changes in seawater chemistry are driven by variations in geological factors such as hydrothermal discharge from the global mid-ocean ridge system, the rate and type of material being terrestrially weathered, dolomitisation, and reverse weathering (e.g. Lowenstein et al., 2014; Coogan and Dosso, 2015; Higgins and Schrag, 2015). Moreover, the major ion chemistry of seawater is in itself a potential tracer of these geochemical processes. Several studies have reconstructed seawater El/Ca with a temporal resolution similar to that of the residence time of Ca^{2+} in seawater using different marine carbonates (Coggon et al., 2010; Delaney et al., 1989; Dickson, 2002; Evans et al., 2018a; Gothmann et al., 2015; Wit et al., 2017). Recently, the Na/Ca ratio of foraminifera calcite has shown to be much more sensitive to changes in $[Ca^{2+}]_{sw}$ than seawater salinity, and given the long residence time of Na^{+} in seawater (~100 Myr; Broecker, 1982), Na/Ca may be interpreted purely in terms of $[Ca^{2+}]_{sw}$ changes (Hauzer et al., 2018; Le Houedec et al., 2021; Zhou et al., 2021). The approach of directly reconstructing $[Ca^{2+}]_{sw}$ using a trace element ratio containing an element with an extremely long residence time suggests the possibility that other elements with a long-term near-constant concentration may offer similar information.

Potassium is a major element in seawater (K_{sw}), with a present-day concentration of 10.2 mmol kg^{-1} and a residence time of ~12 million years (Broecker, 1982). The major source of potassium in the ocean is from riverine input and high-temperature hydrothermal processes, whereas removal of K^{+} from seawater takes places by formation of authigenic clay formation by reverse weathering and low temperature hydrothermal processes (Bloch and Bischoff, 1979; Kronberg, 1985;

45 Michalopoulos and Aller, 1995). The seawater Sr, Li and Os isotope records have been used to argue
46 for a substantial increase in continental weathering through the Cenozoic (particularly the Neogene)
47 (McCauley and DePaolo, 1997; Misra and Froelich, 2012; Raymo and Ruddiman, 1992), although
48 several other processes may impact these systems (e.g. Coogan and Dosso, 2015). Indeed, other
49 processes, such as a decrease in reverse weathering (Dunlea et al., 2017; Higgins and Schrag, 2015;
50 Isson and Planavsky, 2018; Misra and Froelich, 2012), high-temperature hydrothermal processes
51 (Hardie, 1996; Horita et al., 2002), and low-temperature hydrothermal processes (Coogan and Dosso,
52 2015) have also been proposed to have driven seawater chemistry changes over the same interval.

53 Despite evidence for past variability in several processes that are important components of
54 the K cycle, the concentration of K_{sw} has been suggested to have remained relatively constant
55 throughout the Phanerozoic (9-11 mmol kg^{-1}) on the basis of modelling data from fluid inclusions
56 trapped in evaporitic sequences (Horita et al., 2002; Lowenstein et al., 2001). If K_{sw} has indeed
57 remained within narrow bounds, the K/Ca ratio of marine carbonates may be an additional direct
58 tool for the reconstruction of past changes in $[Ca^{2+}]_{sw}$. Moreover, coupling this system with Na/Ca,
59 within a multi-proxy approach, would allow (e.g.) the constancy of Phanerozoic K_{sw} to be verified. To
60 evaluate the potential of K/Ca measurements of marine carbonates for this purpose, we investigated
61 1) two symbiont-bearing species collected from the modern ocean: the low-Mg calcite planktonic
62 foraminifera *Globigerinoides ruber* (white) and the high-Mg calcite, larger benthic foraminifera
63 *Operculina* sp. from globally distributed sites characterised by a wide range in seawater parameters
64 to determine the impact of environmental parameters on K incorporation, 2) cultured *Operculina*
65 *ammonoides* grown at different seawater $[Ca^{2+}]$ and temperature (Hauzer et al., 2018) to determine
66 whether the proxy functions as hypothesised, and 3) cultured *O. ammonoides* grown at different pH

values beyond the modern range, to understand whether the changing seawater carbonate system might influence foraminifera K/Ca. Finally, we compiled literature data of the K/Ca and Na/Ca of a diverse range of biogenic $CaCO_3$ to understand the broader controls on K and Na incorporation.

2. Materials and methods

2.1. Modern foraminifera

Larger benthic foraminifera (LBF) of the genus *Operculina* were hand-sampled from SW Sulawesi, NE Kalimantan, Jakarta Bay, the Gulf of Eilat (*Operculina ammonoides*) and the Great Barrier Reef (*Operculina* sp.) (Tab. 1). These samples have been previously investigated for the purposes of producing a Mg/Ca–temperature field calibration (Evans et al., 2013), with further details of sample collection given in Renema (2006; 2008).

In order to relate shell geochemistry to environmental parameters, mean annual sea surface temperature (SST) and salinity data were taken from the 1° resolution version of the World Ocean Atlas 2018 (Locarnini et al., 2018; Zweng et al., 2019) for all *Operculina* samples except those from the Gulf of Eilat (Eil 19), for which data from the monitoring station of the Interuniversity Institute for Marine Sciences in Eilat (https://www.iui-eilat.ac.il) was used. These samples were earlier measured for Mg/Ca variability along the whorl which coincide with seawater temperature dataset (Evans and Müller, 2013). In contrast to the other sample sites, the Gulf of Eilat is characterised by a large seasonal variability in temperature. Given that the samples analysed here represents the last ~6 months, the November–April mean was used, i.e. the six-month period before the sample collection date. (for detailed information, see Evans et al., 2013). In order to determine the possible influence of the seawater carbonate system on shell geochemistry, the nearest available pH values were taken from Gregor and Gruber (2021). Seawater [CO_3^{2-}] was calculated using CO2sys_v3.0 (Pierrot et al., 2021)

using the *in situ* temperature and salinity from the WOA and total alkalinity (TAlk) as the second carbonate system parameter, taken from Gregor and Gruber (2021). The dissociation constants for $KHSO_4$ from Dickson et al., (1990) and the total boron–salinity relationship by Lee et al., (2010) were used. The values of the carbonate system dissociation constants K_1 and K_2 were those from Lueker et al., (2000). The larger benthic foraminifera investigated in this study span a range in seawater temperature, salinity, pH, and [CO_3^{2-}] ranging from 21.9 to 28.5°C, 32.4 to 40.7 on the practical salinity scale, 8.05 to 8.19 pH units and 207.2 to 284.1 µmol kg^{-1}, respectively (Tab. 1).

Globigerinoides ruber (white) were sampled from sediment traps in the Arabian Sea (AS02-M5) and Bay of Bengal (NBT-09, CBBT-06, and SBBT-09). These samples have been previously investigated for the purposes of refining the Mg/Ca-temperature calibration by Gray et al. (2018). Foraminifera were picked from the 200 to 400 µm size fraction. Temperature and salinity used in this study are the same as those reported in Gray et al. (2018) (Tab. 1). In addition, we analysed *G. ruber* (white) from a globally-spaced set of core-top samples which have been previously investigated to better understand B/Ca as a potential carbonate system proxy (Henehan et al., 2015). These foraminifera were picked from the 300-350 µm size fraction except for sample MC420, which was picked from the 355-400 µm fraction. Temperature and salinity used to relate shell geochemistry are those reported in Henehan et al. (2015) (Tab. 1). *In situ* carbonate chemistry data have been previously reported from both the sediment trap and core to sample sets utilized here, but were calculated in different ways. To ensure consistency in data treatment, the carbonate system parameters were therefore recalculated here. The [CO_3^{2-}] values was calculated using CO2sys_v3.0 (Pierrot et al., 2021) taking the nearest available pH and TAlk values from Gregor and Gruber (2021). The constants of Lueker et al., (2000), Lee et al., (2010), and Dickson et al., (1990) were used. The sample location

details of all *G. ruber* measured in this study are given in Tab. 1. Together, the planktonic foraminifera investigated in this study from both sediment traps and core tops span a range in seawater temperature, salinity, pH, and [CO_3^{2-}] ranging from 22.0 to 28.7°C, 32.7 to 36.4 on the practical salinity scale, 8.05 to 8.12 pH units (total scale) and 204.1 to 238.8 µmol kg^{-1}, respectively (Tab. 1).

Tab. 1. Sample site details of the modern foraminifera analysed here.

i) Larger Benthic foraminifera; all species are *Operculina ammonoides* except SS 07G14 (*Operculina* sp.)

Sample ID	latitude	longitude	Water depth (m)	T (°C)	1 SD	S	1 SD	pH (total scale)	1 SD	$[CO_3^{2-}]$* (µM)	1 SD	n
Pd 2805[a]	-5.03	119.33	20	28.0	1.1	33.4	0.9	8.06	0.02	209.0	11.2	4
KKE30[b]	-5.11	119.29	30	27.7	1.1	33.5	0.9	8.06	0.02	208.2	11.3	5
SER 33[c]	-5.86	106.7	14-24	28.5	0.8	32.4	0.8	8.07	0.02	212.1	10.3	4
SS 07G14[b]	-19.73	150.22	74	24.9	1.0	35.3	0.2	8.09	0.03	219.9	14.4	7
Eil 19[b]	29.54	34.97	10-15	21.9	0.8	40.7	0.1	8.19	0.02	284.1	14.2	7
BBx 49A[b]	1.39	118.82	48	27.8	0.9	34.2	0.2	8.05	0.02	207.2	10.0	8
Pd 2801[a]	-5.03	119.33	20	28.0	1.1	33.4	0.9	8.06	0.02	209.0	11.2	4

ii) Planktonic foraminifera (*Globigerinoides ruber*)

Sample ID	latitude	longitude	Water depth (m)	T (°C)	1 SD	S	1 SD	pH (total scale)	1 SD	$[CO_3^{2-}]$* (µM)	1 SD	n
NBBT-09 No.5[d]	17.38	89.70	1450	27.1	1.0	32.7	0.7	8.07	0.02	204.1	11.3	5
CBBT-06 No.9[d]	11.03	84.43	899	28.6	0.5	33.8	0.3	8.07	0.02	217.2	9.5	9
SBBT-09 No.4[d]	5.40	86.77	886	28.2	0.4	34.3	0.3	8.06	0.01	219.4	8.9	10
SBBT-09 No.2[d]	5.40	86.77	886	28.2	0.3	34.3	0.2	8.06	0.01	219.1	8.8	10
AS02-M5 No.4[d]	10.00	65.01	2363	27.2	0.6	36.1	0.4	8.06	0.01	229.6	10.1	9
AS02-M5 No.12[d]	10.00	65.01	2363	28.7	0.4	36.0	0.2	8.06	0.01	238.8	10.1	10
MC423[e]	17.75	-65.59	1813	27.5	1.0	35.6	0.4	8.07	0.02	231.2	12.5	10
MC420[e]	17.04	-66.00	4705	27.6	0.5	35.5	0.2	8.07	0.02	229.4	11.4	10
MC497[e]	23.53	63.31	1000	26.9	1.8	36.4	0.1	8.05	0.02	227.4	14.8	10
G4[e]	-28.42	167.25	831	22.0	2.0	35.8	0.1	8.12	0.02	218.3	15.4	10

a:Renema, 2002; b: Evans et al., 2013; c: Renema, 2008; d: Gray et al., 2018; e :Henehan et al., 2015; *derived using CO2Sys_v3.0 (see text for detail); n= no. of sample analysed; T= temperature; S=salinity

2.2. Cultured foraminifera

We investigated two sets of laboratory culture experiments in which *Operculina ammonoides* were grown at: 1) varying seawater Ca^{2+} concentration, repeated for three sets of temperature, and 2) varying seawater pH at constant DIC. Details of the culture procedure are given in Evans et al., (2015), Hauzer et al., (2018) and Hauzer, (2022). Briefly, live *O. ammonoides* from the 475-690 µm size fraction were collected from the North Beach, Eilat, Israel, at a depth of ~20-25 m. Prior to the experiment, foraminifera were placed in seawater labelled with the fluorescent marker calcein (50 µM) for 4-5 days and those that showed at least one fluorescent chamber were then transferred to seawater with the desired experimental conditions. The culture seawater medium was additionally spiked with 0.15 µM $BaCl_2$ solution (74 nM ^{135}Ba) in order to unambiguously identify newly precipitated calcite (Evans et al., 2016). Foraminifera grown under the culture conditions typically had between 3-13 non-fluorescent chambers grown after the calcein mark (Hauzer et al., 2018). These specimens were selected for further analysis; only data from chambers characterised by $^{135}Ba/^{138}Ba$ higher than the natural abundance were considered in our data analysis.

The culture experiment with varying $[Ca^{2+}]_{sw}$ used in this study is the same as that described in Hauzer *et al*. (2018) and Hauzer (2022), and was originally performed to determine the sensitivity of Na, Mg, Sr and Li incorporation into *O. ammonoides* to changing $[Ca^{2+}]_{sw}$, with the principal aim of establishing Na/Ca as a proxy for past changes in $[Ca^{2+}]_{sw}$. Comprehensive details of the experiment are given in Hauzer et al., (2018). The seawater calcium concentration was modified by adding $CaCl_2$, resulting in $[Ca^{2+}]_{sw}$ of 10.7, 12.7, 15.3, and 18.0 mmol kg^{-1}. Given that calcification in the culture jars results in lower TAlk and DIC, the seawater carbonate chemistry was monitored and

replaced regularly in order to maintain quasi-constant conditions. This experiment was conducted at three different temperatures: 22°C, 25°C, and 28°C.

The culture experiment at varying pH with constant DIC was conducted by modifying the TAlk of natural Gulf of Eilat seawater to the desired values by addition of HCl and NaOH (Hauzer, 2022, also see Evans *et al.*, 2018 for further experimental details). As in the case of the $[Ca^{2+}]_{sw}$ experiment, the seawater was changed at regular intervals in order to, as far as possible, maintain constant conditions. pH and TAlk were monitored throughout the experimental period in both the culture jars as well as the seawater reservoirs, enabling us to report our trace element data against average measured values throughout the course of the experiments. Seawater pH, adjusted via changing the seawater TAlk at constant DIC, was experimentally varied between 7.5 to 8.3 (NBS scale). The saturation state (Ω_c), calculated using CO2sys using TAlk and pH measured during experimental period showed variability between 1.3 to 8.5 (Tab. S6).

At the end of both experiments, the foraminifera were cleaned with deionised water, treated with 1.5% NaOCl overnight to remove any organic material present, and then washed thoroughly several times with deionised water.

2.3. LA-SF-ICPMS analysis

Prior to analysis, all foraminifera were treated once again with 10% sodium hypochlorite (NaOCl) to oxidise any possible remnant organic material. The samples were then rinsed 3–4 times by ultrasonication in 18.2 MΩcm deionised water, followed by a final ultra-sonication cleaning step in methanol. The sample mounting procedure of the foraminifera in the laser ablation cell differed depending on the species being analysed. Each larger benthic foraminifera was mounted by placing it into pressure-sensitive adhesive. Cultured specimens were placed vertically to target the marginal

cord and the newly formed chambers were ablated starting from the final chamber and working backwards (3-5 chambers total). Most (modern) field-collected LBF specimens were placed horizontally in order to measure the knobs (pustules) (see Fig. 2), while some were analysed on both the knob regions and the marginal cord, in order to compare the data derived from the two areas. In general, the knobs were targeted where possible (i.e. in modern samples) because the calcite in this region is non-porous, unlike the marginal chord, thus minimizing the risk of contamination from sedimentary particles (see Sec. 3.2 for further details). Planktonic foraminifera were placed directly onto double-sided carbon tape with the umbilical side down, allowing the final three chambers to be ablated.

Trace element measurements were performed using a sector-field ICP-MS (Thermo Element XR) combined with a RESOlution 193 nm ArF laser ablation system equipped with a Laurin Technic S-155 two-volume laser-ablation cell (see Müller et al., 2009) at the Frankfurt Isotope and Element Research Center (FIERCE), Goethe University Frankfurt. Ablation was carried in an atmosphere of He and Ar with an additional diatomic gas, N_2, added downstream of the ablation cell. The instrument was tuned for maximum sensitivity while maintaining Th/U between 0.9-1.0 and ThO^+/Th^+ <1 %. The detailed operating parameters of the LA and ICPMS setup as applied specifically to this study are described in Tab. S1. Monitored masses (m/z) were ^{23}Na, ^{24}Mg, ^{25}Mg, ^{27}Al, ^{39}K, ^{43}Ca, and ^{55}Mn, with Al/Ca and Mn/Ca used to check that sample cleaning removed all remnant sedimentary particles and that there were no diagenetic overgrowths. Standardisation of the data followed established protocols (Heinrich et al., 2003), using ^{43}Ca as the internal standard and the NIST SRM610 glasses as the external standard, analysed in an identical manner to the samples. Data reduction was performed using an in-house Matlab script (Evans and Müller, 2018) which automatically identifies sample and

gas blank data, subtracts the latter from the former, and calibrates trace element ratios using a depth-dependent measured/reported element/^{43}Ca ratio derived from repeat analysis of the NIST SRM61x glasses.

Planktonic foraminifera were analysed in high mass resolution mode (Δm/m = 10,000) whereas the larger benthic foraminifera were analysed in medium mass resolution (Δm/m = 4000). Although high-resolution is required for complete resolution of ArH^+ on K^+ and was initially used to assess whether sufficient data quality could only be achieved when these are fully separated, we observed that medium-resolution is sufficiently capable of minimizing the effect of the ArH^+ interference (Fig. S1), such that we chose medium-resolution for most of the measurements that we report here as the best trade-off between separation of $^{38}ArH^+$ and $^{39}K^+$ and sensitivity. All samples were calibrated using sample-standard bracketing by analysing NIST SRM610 under identical conditions to the samples every ~20-30 minutes (i.e., blocks of ~10 analyses). The reported NIST SRM610 values of Jochum et al., (2011) were used with the exception of Mg, for which we use that of Pearce et al., (1997) following the recommendation of Evans and Müller, (2018). The MPI-DING komatiite glass GOR-128G (Jochum et al., 2006) and the nanopellet form (Garbe-Schönberg and Müller, 2014; Jochum et al., 2019) of the carbonate standard JCp-1 (Okai et al., 2002) were measured at random intervals within the sequence using the same analytical conditions in order to assess the accuracy and precision of our sample data.

The accuracy of Mg/Ca, Sr/Ca, Al/Ca, and Mn/Ca in GOR-128G were within ±5%, whereas accuracy for Na/Ca and K/Ca was around 10.9% and 10.3% respectively. The higher offset from the true value in GOR-128G in the case of the alkali elements has previously been shown to be a result of a difference in the down-hole fractionation factor for the alkali metals in the GOR glass standards

with respect to NIST SRM610 (Evans and Müller, 2018). This is demonstrated by the fact that our long-term Na/Ca accuracy is <5% in JCp-1, which was also the case for Al/Ca, Sr/Ca and Mg/Ca, whereas our Na/Ca and K/Ca data in GOR-128G are inaccurate to a similar degree. Assessing the accuracy of K/Ca measurements by LA-ICPMS is challenging because few $CaCO_3$ secondary standard materials exist. We measure a long-term average value of JCp-1 that is offset by 8.6% from that given by Okai et al., (2002), determined by Atomic Absorption Spectroscopy, but we do not apply an accuracy correction to our data because this reported value is based on a measurement from one laboratory. Nonetheless, it is possible that an accuracy correction on our data of the order of ~9% may be warranted in future if the value of Okai et al., (2002) is reproduced in other laboratories and/or in other test portions of the JCp-1 powder. Precision estimated from repeat measurement of these two secondary standards across the full analytical period represented here (~2 years) was <6% for all element/Ca ratios in GOR-128G (2σ). The precision for K/Ca, Mg/Ca and Sr/Ca in our JCp-1 nanopellet was less than 7% (2σ), whereas Na/Ca and Al/Ca precision was ~10% (2σ), which we attribute to the lower concentration and possible presence of minor inhomogeneities in this standard material. Precise details of data quality are given in Tab. S2.

3. Results

3.1. Influence of seawater parameters on K incorporation in *Globigerinoides ruber* (white)

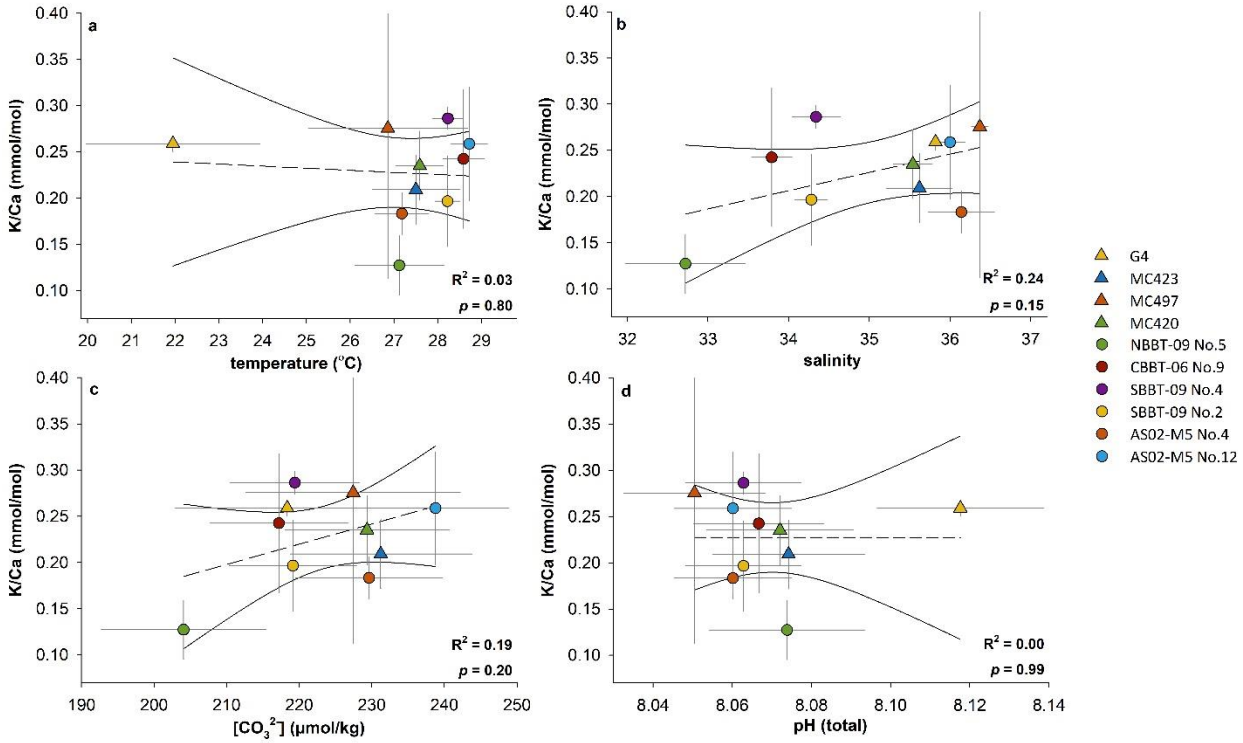

Fig. 1. K/Ca values of modern *G. ruber* plotted against a) temperature, b) salinity, c) [CO_3^{2-}] and d) pH. Sediment trap-collected foraminifera are depicted with circles and core top foraminifera with triangles. All error bars are 1SD. The solid line represents the 95% confidence interval on the linear regressions. Sample site details are given in Tab. 1.

The Al/Ca and Mn/Ca of all the planktonic foraminifera were lower than 0.15 mmol mol^{-1} (Tab. S3), demonstrating that contamination from remnant detrital material, if present, was effectively removed by our cleaning procedure. The mean value of K/Ca in *G. ruber* from sediment-trap samples (0.22±0.05 mmol mol^{-1}) and core-top (0.24±0.03 mmol mol^{-1}) samples are statistically indistinguishable based on a Student's t-test at the 95% confidence interval, such that we combine both datasets together. The similarity in the mean value of *G. ruber* K/Ca measured in core-top samples and sediment trap samples suggests minimal to no effect of early-stage diagenesis. The K/Ca in modern *G. ruber* ranges from 0.13 to 0.29 mmol mol^{-1} (Fig. 1; Tab. S3). We find no significant

relationship between K/Ca and temperature (R^2 = 0.03; p = 0.80), salinity (R^2 = 0.24; p = 0.15), [CO_3^{2-}] (R^2 = 0.19; p = 0.20), or pH (R^2 = 0.00; p = 0.99). Multiple linear regression analysis of K/Ca against all possible combinations of pH, temperature, [CO_3^{2-}], and salinity also yielded no statistically significant relationship, demonstrating no resolvable influence of seawater composition on K incorporation into the shells of this species. However, considering only sediment trap samples, a significant relationship of K/Ca with temperature is observed (m = 0.068, R^2 = 0.66; p = 0.049).

3.2. Influence of seawater parameters on K incorporation in *Operculina ammonoides* collected from the modern ocean

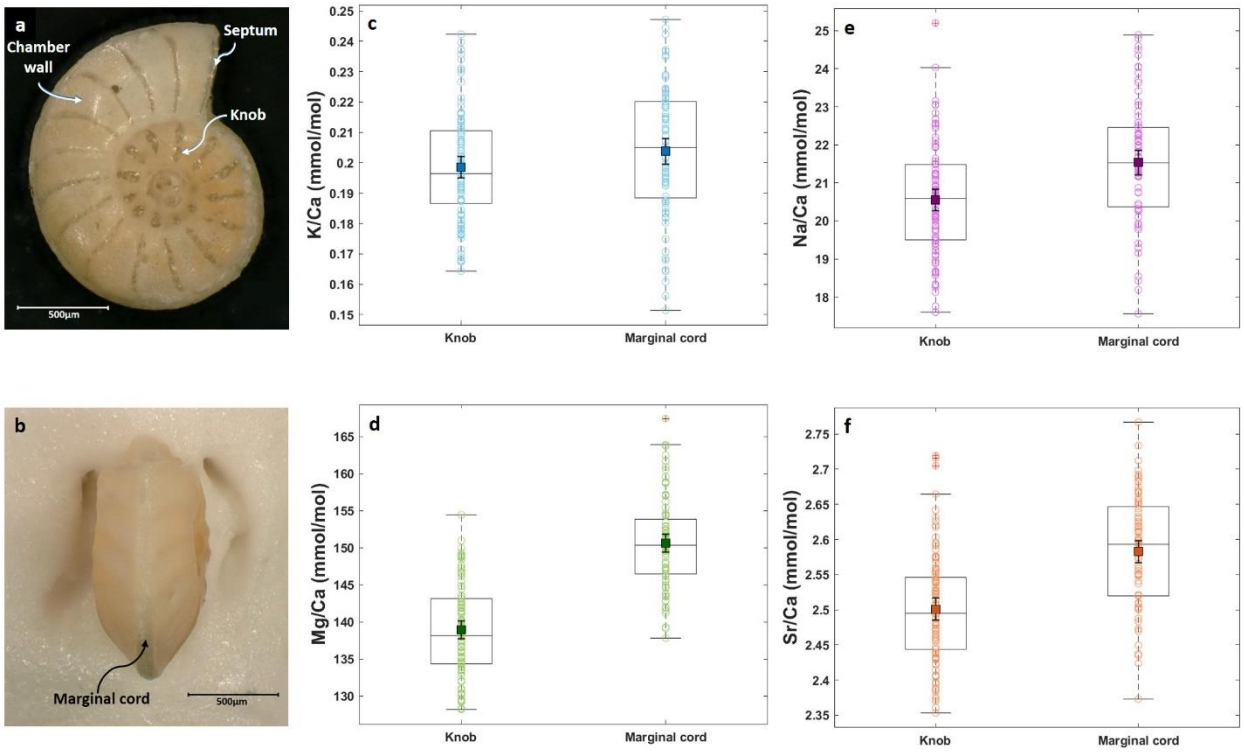

Fig. 2. Possible intra-shell element heterogeneity of *Operculina ammonoides* investigated using samples from the Gulf of Eilat (Eil 19). a,b) Representative specimens of *Operculina ammonoides* showing the regions of the shell investigated here (knob areas and marginal cord). c-f) Box plots of the measurements performed on knobs (n=18) and marginal cord (n=13). Each open circles represents an individual ablated spot. Filled squares shows the average value. Error bars on the average values are 2SE.

The larger benthic foraminifera *O. ammonoides* forms a complex shell structure with several distinct structural components (Carpenter, 1862; Hohenegger, 2011), consisting of septa, chamber

250 walls, knob structures, and the marginal cord (see Fig. 2). To first understand whether measured trace
251 element ratios in *O. ammonoides* are sensitive to the choice of which part of the shell is being
252 analysed, i.e. to investigate possible heterogeneity in shell geochemistry, and given that elemental
253 banding in the chamber wall of benthic foraminifera (including K/Ca) has been reported (Geerken et
254 al., 2019), we analysed both the marginal cord (porous) and knob (non-porous) regions of *O.*
255 *ammonoides* from the Gulf of Eilat (sample Eil 19; Fig. 2). In addition, we investigated Mg/Ca, Na/Ca
256 and Sr/Ca to compare the variability in their elemental ratios in these two regions of the shell, to
257 understand whether trace element data from this species is sensitive to the region analysed. While
258 we do observe ±20% K/Ca variability between individual laser spots (Fig. 2), the K/Ca ratio of the
259 knobs (0.199±0.004 mmol mol^{-1}) and marginal cord (0.205±0.005 mmol mol^{-1}) are statistically
260 indistinguishable based on a Student's t-test at the 95% confidence interval. The difference in the
261 average value of Sr/Ca in both regions was 3.2%, whereas the average Na/Ca and Mg/Ca values
262 were about 4.6% and 7.8% higher along the marginal cord, respectively (Fig. 2). Marginally higher
263 values of Mg/Ca along the marginal cord have been previously reported (Evans et al., 2015). While
264 this demonstrates that a consistent choice regarding the part of the shell to be analysed should be
265 made in the case of Na, Mg, and Sr, the same is not true in the case of K/Ca. Hence, we performed
266 all measurements on the non-porous knob region in all modern LBF to minimise possible
267 contamination.

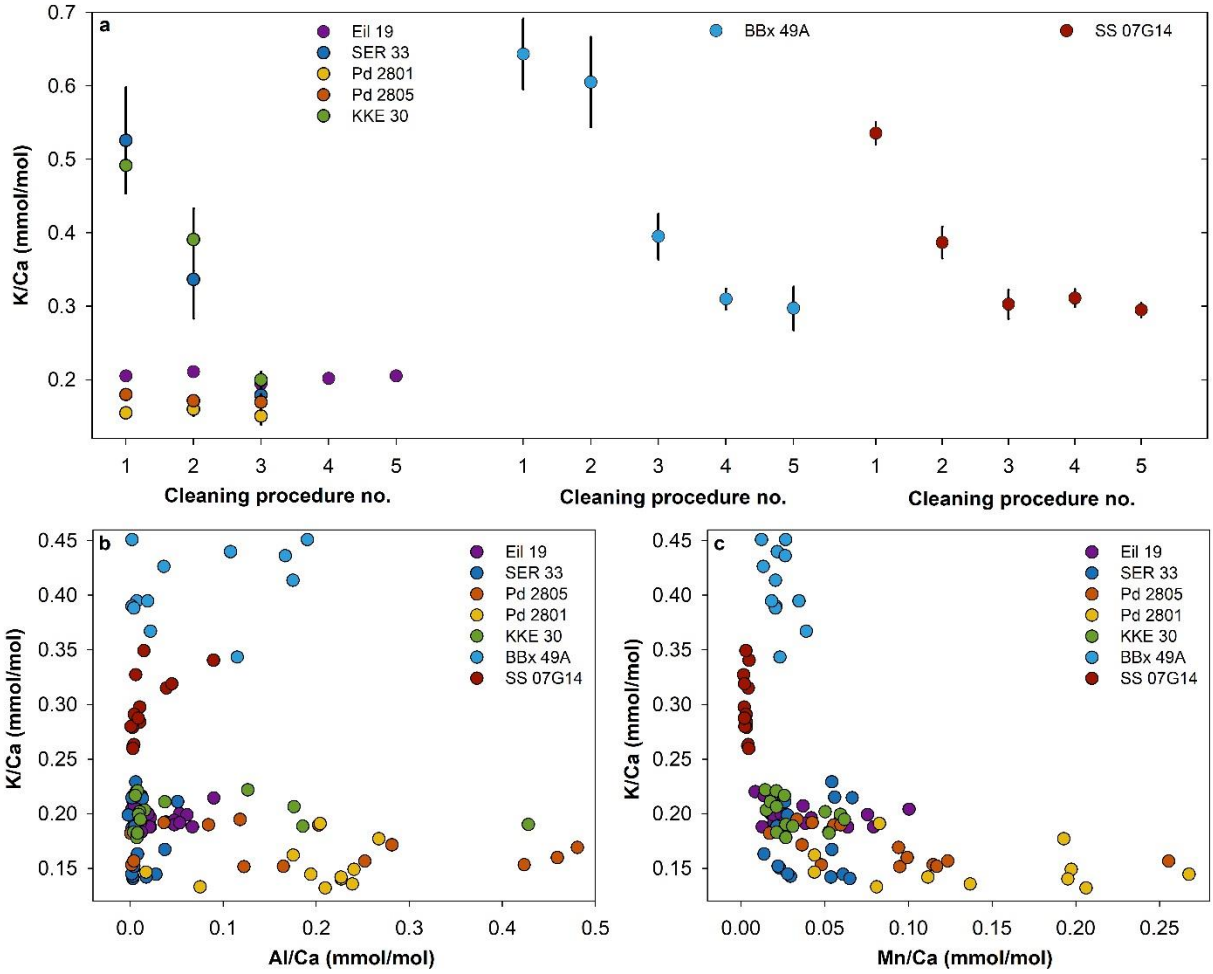

Fig. 3. a) Variation in K/Ca values during repeated cleaning steps (step 1: 10% NaOCl + methanol + deionised water; step 2-5: methanol + deionised water). The relationship of K/Ca in modern *Operculina* sp. with b) Al/Ca and c) Mn/Ca following the final cleaning process (see Methods).

The K/Ca measurements performed on *Operculina* sp. were repeated 3-5 times after repeated cleaning procedures (in addition to those described in the Methods section) to assess whether the initial cleaning steps were sufficient to remove all contaminant phases from the shell. This additional cleaning step consisted solely of a further ~10-15 minute ultrasonication in methanol followed by several deioinised water (18.2 MΩcm) rinses. Further oxidative cleaning steps were not conducted because we suspect that possible remnant contaminant phases are sedimentary particles that require physical removal, rather than the result of (e.g.) incomplete oxidation of organic material.

279 Al/Ca and Mn/Ca were monitored to determine contamination-free measurements after each
280 cleaning step, and the overall change in K/Ca after each sequential step was used to determine
281 whether incomplete removal of possible contaminant phases during this process biased the mean
282 sample values. We observe a decrease in measured K/Ca in the first three cleaning steps in four out
283 of the seven samples investigated here, indicating that a single oxidative cleaning step followed by
284 several deioinised water rinses is unlikely to be sufficient to remove K contamination in the majority
285 of cases, even when analysing non-porous regions of the shell. Specifically, samples Pd 2801, Pd
286 2805, and Eil 19 were characterised by no significant change in K/Ca with further cleaning, whereas
287 SS 07G14, KKE 30 and SER 33 needed three additional cleaning steps (Fig. 3a). The K/Ca of *Operculina*
288 from NE Kalimantan (BBx 49A) continued to decrease even after the third cleaning step (Fig. 3a). The
289 decrease in the K/Ca after cleaning step-2 represents possible clay contamination. . Even after five
290 cleaning steps the K/Ca of BBx 49A and SS 07G14 remained substantially elevated compared to the
291 other larger benthic foraminifera samples, but we retain both in our data analysis because there is
292 no reason to treat these data points as outliers. After the final cleaning step, all samples that were
293 considered in this study were characterised by Al/Ca and Mn/Ca lower than 0.5 mmol mol^{-1} and 0.3
294 mmol mol^{-1}, respectively (Fig. 3b,c). Due to higher Al/Ca, we had to remove one foraminifera each
295 from Pd 2805, Pd 2801, and BBx 49A.

296 Within the subset of samples that were unambiguously not affected by remnant
297 contamination, K/Ca in modern *Operculina* sp. varied between 0.15±0.01 mmol mol^{-1} to 0.31±0.01
298 mmol mol^{-1} (Tab. S4). The relationship between K/Ca in modern *Operculina* sp. and key
299 oceanographic parameters is shown in Fig. 4. These data demonstrate that there is no clear
300 relationship between K/Ca in modern *Operculina* and temperature, salinity, $[CO_3^{2-}]$ or pH (R^2 of K/Ca

versus temperature, salinity, [CO_3^{2-}] and pH were 0.07, 0.02, 0.00, and 0.00, respectively), implying no resolvable influence of these seawater parameters on K incorporation in *Operculina* species, although we note that the addition of further modern data is a priority, given the relatively small sample number.

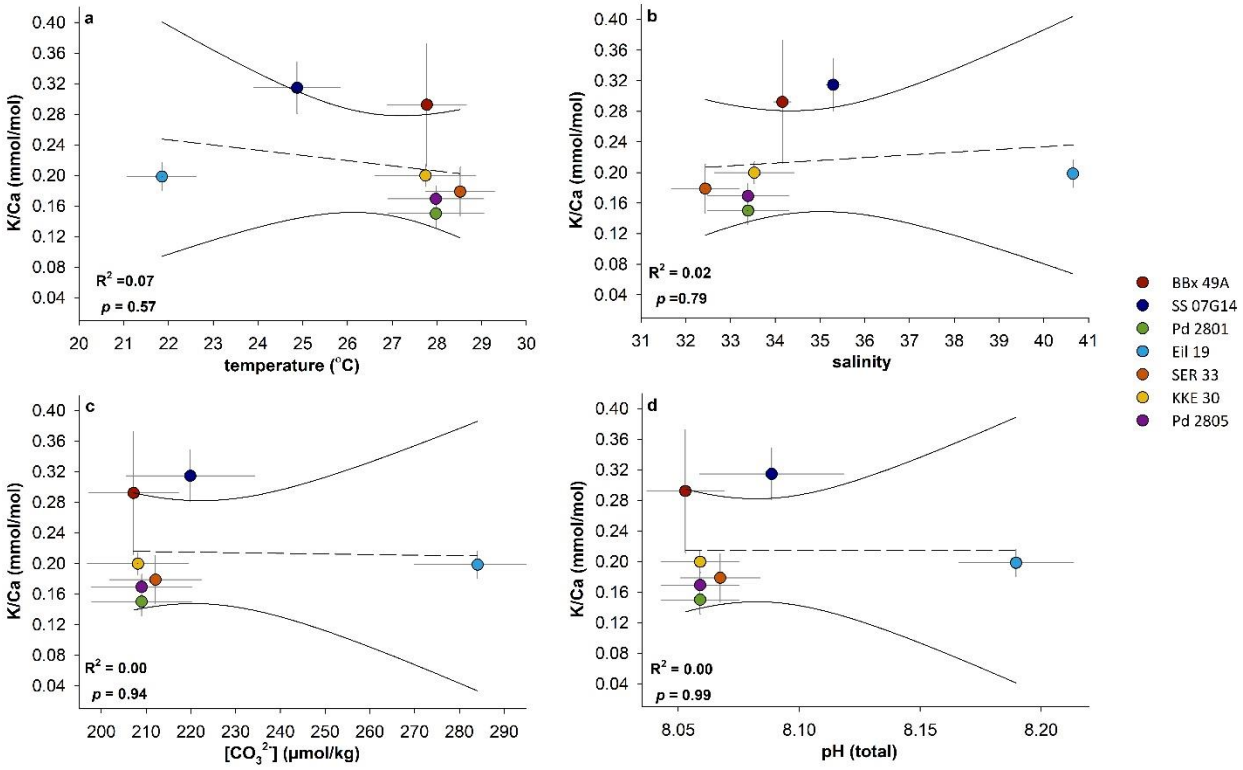

Fig. 4. K/Ca in modern *Operculina* sp. as a function of temperature, salinity, pH, and [CO_3^{2-}]. All error bars are 1SD. The solid line represents the 95% confidence interval on the linear regressions. Sample site details are given in Tab. 1.

3.3. Incorporation of K in cultured *Operculina ammonoides* grown in seawater with variable $[Ca^{2+}]_{sw}$ and variable pH

O. ammonoides were cultured at three different temperatures and four different $[Ca^{2+}]_{sw}$ (12 experiments in total, (see Hauzer et al., (2018)). The K/Ca of *O. ammonoides* grown at elevated $[Ca^{2+}]_{sw}$ were broadly reproducible irrespective of the culture temperature. For example, at the highest $[Ca^{2+}]_{sw}$ value investigated here (18 mmol kg^{-1}), K/Ca = 0.180±0.016, 0.193±0.017, and

316 0.195±0.013 mmol mol^{-1} at 28, 25, and 22°C respectively (Fig. 5a; Tab. S7). The exception to this was
317 the lowest $[Ca^{2+}]_{sw}$ experiment (10.7 mmol kg^{-1}, equivalent to modern seawater at salinity = 37), in
318 which K/Ca was 0.189±0.018, 0.210±0.010, and 0.261±0.009 mmol mol^{-1} at 28, 25, and 22°C
319 respectively (Fig. 5a). However, the K/Ca of cultured foraminifera overall falls within the range of the
320 modern field samples described above, in which we find no clear relationship between K
321 incorporation and seawater temperature, salinity, or carbonate chemistry. As such, we pool the data
322 together from the three temperature experiments conducted for each $[Ca^{2+}]_{sw}$ (Tab. S5), treating the
323 three experiments as replicate cultures at a given $[Ca^{2+}]_{sw}$ to examine the overall relationship between
324 seawater and shell K/Ca. The average K/Ca_{LBF} values are tightly correlated with $[Ca^{2+}]_{sw}$, albeit with a
325 very shallow slope (the least squares linear regression has m = 0.072±0.013). Because the shell K/Ca
326 ratio must equal 0 at K/Ca_{sw} = 0, we fit a distribution function through the data (see Hauzer et al.,
327 (2018) for terminology). This yields a power relationship ($y=ax^b$) with K/Ca_{sw} (b = 0.29, R^2 = 0.93, p =
328 0.04), again, with a shallow slope compared to other major/trace elements (Na/Ca: b = 0.54; Mg/Ca:
329 b = 0.72; Evans et al., (2015); Hauzer et al., (2018)).

330 The Na/Ca data of this study are a test of analytical external reproducibility, given that Na/Ca
331 of the same samples was previously reported by Hauzer et al. (2018), measured in a different
332 laboratory and using a different type of mass spectrometer. Our LA-SF-ICPMS results agree well with
333 the previously reported LA-Q-ICPMS Na/Ca data (Fig. 5b), demonstrating that a power function
334 between Na/Ca_{sw}-Na/Ca_{shell} best describes the culture experiment. This adds confidence to the inter-
335 laboratory comparability of laser ablation trace element data using different mass spectrometers
336 (note that the data reported here use NIST SRM610 as a primary calibration standard, whereas
337 Hauzer et al. (2018) used NIST SRM612 for Na/Ca quantification).

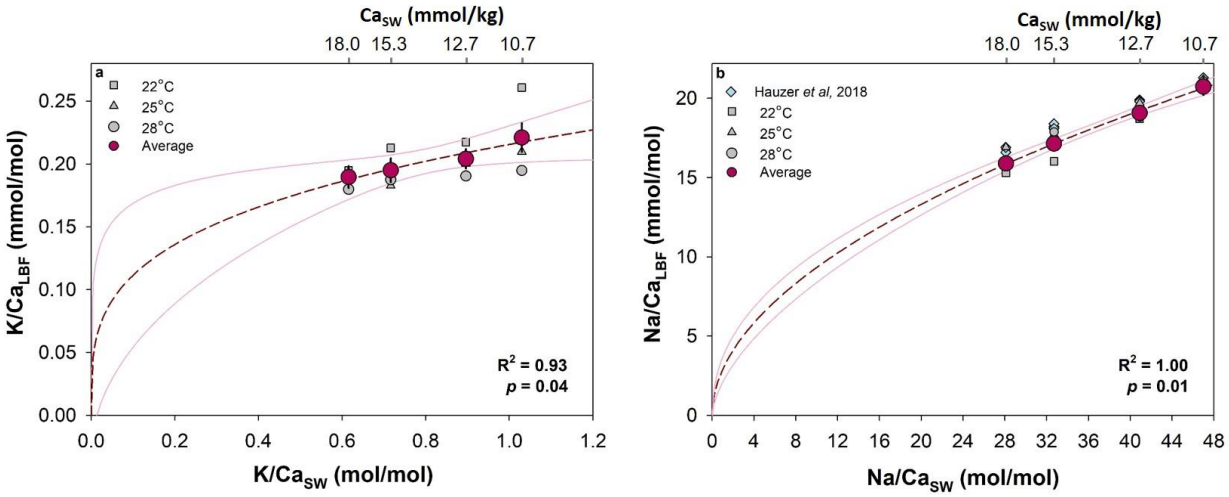

338

339 **Fig. 5.** a) The relationship between *Operculina ammonoides* and seawater K/Ca. b) The relationship between
340 *Operculina ammonoides* and seawater Na/Ca. Error bars represent 2SE. The solid line represents the 95%
341 confidence interval on the power regressions. The seawater Ca_{sw} values are taken from Hauzer et al., (2018)

342 Measured K/Ca values in foraminifera grown at different pH (constant DIC) are shown in Fig.
343 6, with the data reported in Tab. S6. Although we find no resolvable relationship between K/Ca and
344 pH in the modern *O. ammonoides* samples (Fig. 4), K/Ca and pH shows significant relationship in this
345 culture experiment (R^2 = 0.96; p = 0.01), conducted over a much larger pH range (~7.5 to 8.3) (Fig.
346 6a). The saturation state (Ω_c) of the experimental seawaters was estimated using the Matlab program
347 CO2SYS.m (Van Heuven et al., 2011) using the total alkalinity (TAlk) and pH measurements made
348 during experimental period. This exercise demonstrates that a significant relationship exists between
349 *O. ammonoides* K/Ca and seawater saturation state (Ω_c) (R^2 = 0.96; p = 0.01; Fig. 6b), with a slope of
350 0.0067 mmol mol^{-1} per unit change in Ω_c.

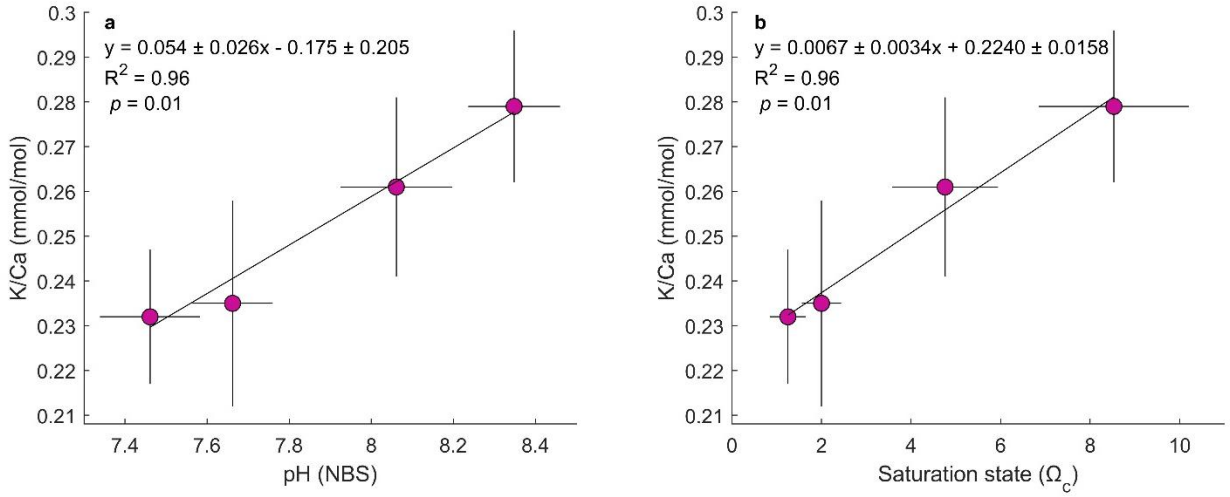

Fig. 6. The relationship between K/Ca in cultured *O. ammonoides* and a) pH and b) saturation state (Ω_c). The equation represents the York-fit linear regression line (solid line), accounting for the uncertainties in both axes (York et al., 2004). R^2 and *p* values represents least square fit line. Error bars are 2SE.

4. Discussion

4.1. Controls on modern high-Mg benthic and low-Mg planktonic foraminifera K/Ca

We investigated the effect of a wide range of seawater carbonate chemistry and physical parameters on K/Ca in both the shallow dwelling, warm water high-Mg calcite larger benthic foraminifera (*Operculina sp.*) and the low-Mg calcite planktonic foraminifera (*G. ruber*). The contrasting mineralogy of these species, as well as the wide range of ambient conditions investigated here in both laboratory culture and the natural environment, means that the sample set is well-placed to identify whether any of these factors drive changes in K incorporation.

With regards to the effect of mineralogy, we observe Na/Ca 2-3 times higher in the high-Mg foraminifera than the low-Mg foraminifera, as previously reported (e.g. Delaney et al., 1985; Evans et al., 2015; van Dijk et al., 2017; Bertlich et al., 2018). This has been previously ascribed to Mg-induced lattice distortion (Evans et al., 2015; Hauzer et al., 2018), while the presence of Na at relatively high concentration in organic-rich layers within the shell has also been described (Bonnin et al., 2019; Branson et al., 2016). In contrast to Na (and Sr; Mucci and Morse, (1983); Evans et al., (2015)), we

observe that the average value of K/Ca in modern high-Mg foraminifera *Operculina* sp. (0.21±0.02 mmol mol^{-1}) falls in the same range as the average of all modern low-Mg planktonic species *G. ruber* (0.23±0.03 mmol mol^{-1}). This possibly suggests a similar incorporation mechanism of K in these foraminifera and/or no effect of mineralogy on the K distribution coefficient.

Previous work has shown that salinity exerts a control on the incorporation of alkali ions (i.e., Na and Li) in both biogenic marine carbonates and inorganic calcite (Allen et al., 2016; Hauzer et al., 2021; Marriott et al., 2004; Wit et al., 2013). For example, the effect of salinity on alkali element incorporation in *O. ammonoides* was observed to be 1.38% per salinity unit in the case of Na/Ca and 2.05% for Li/Ca (Hauzer et al., 2021). The effect of salinity on *G. ruber* Na/Ca appears to differ between plankton-tow and core-top samples, and/or depending on how the samples are analysed (laser ablation versus solution ICPMS). For example, Allen et al., (2016) report a 1.09% change in Na/Ca per salinity unit in laboratory culture measured by solution ICPMS, whereas Mezger et al., (2016) report a slope of 0.57 (plankton-tow samples measured by LA). In this study, we observed no relationship between K/Ca and salinity in *O. ammonoides* and *G. ruber*. While we cannot rule out that a salinity control exists, e.g., if a wider range of salinities were to be investigated, this – at least – indicates that other factors readily mask any salinity control on K incorporation in foraminifera.

We find no significant relationship between pH or [CO_3^{2-}] and K/Ca in modern (sediment trap/core-top) *G. ruber* or *O. ammonoides*. Laboratory culture experiments have previously demonstrated no carbonate system control on Li/Ca and Na/Ca in *G. ruber* (Allen et al., 2016), suggesting that seawater carbonate chemistry is not a first-order control on alkali element incorporation in any of these foraminifera in their natural environment. In contrast, we do find a positive relationship between K/Ca and pH in laboratory cultures of *O. ammonoides* conducted over

391 a much wider pH range than that of the modern ocean (Fig. 6a), and some previous studies have
392 demonstrated a Li/Ca sensitivity to the carbonate system in other species (Roberts et al., 2018; Vigier
393 et al., 2015). There is also a significant relationship between K/Ca and the seawater saturation state,
394 discussed in more detail below (Sec. 4.3).

395 Overall, we show that the K/Ca ratio of modern *Operculina* sp. and *G. ruber* is similar, and in
396 both cases not resolvably driven by any key oceanographic parameters or the carbonate chemistry
397 of seawater, to the extent that these vary in the modern (sub)tropics.

398 Finally, we note that the absolute K/Ca ratios that we report for *G. ruber* are ~0.1 mmol mol^{-1}
399 higher than the four planktonic foraminifera samples reported by Li et al., (2021); further data will
400 be required to understand whether this represents real variability in natural samples greater than
401 that reported here, or if it is an artefact of the different analytical or sample preparation procedures.

402 **4.2. Sensitivity of foraminiferal K/Ca to seawater K/Ca**

403 The laboratory culture experiments were conducted at $[Ca^{2+}]_{sw}$ of 10.7, 12.7, 15.3, and 18.0
404 mmol kg^{-1}, with repetitions of each experiment at three temperatures (22°C, 25°C, and 28°C). We
405 observed similar K/Ca for all temperature experiments in the three experiments with elevated
406 $[Ca^{2+}]_{sw}$, whereas in the control experiment with normal $[Ca^{2+}]_{sw,}$ K/Ca of *O. ammonoides* grown at
407 22°C was higher than that at 25°C and 28°C. It is not clear why the lower temperature and low $[Ca^{2+}]_{sw}$
408 favoured the higher incorporation of K/Ca in this foraminifera. Although foraminifera in this
409 experiment were characterised by the lowest growth rates of the set overall (Hauzer *et al.*, 2018) such
410 that this may relate to physiological stress. The modern *ammonoides* sp. datasets presented here
411 suggest that temperature is unlikely to play a substantial role in K incorporation given that, if

412 temperature were the controlling factor, we would also expect to see this effect at cultures conducted
413 under elevated $[Ca^{2+}]_{sw}$.

414 Averaging the results of the three temperature experiments together (Fig. 5), results in a
415 significant but extremely shallow relationship between K/Ca_{shell}-K/Ca_{sw}; to our knowledge, shallower
416 than other trace element reported so far for the surface-dwelling foraminifera (e.g. Li, Mg, Sr, Ba;
417 Delaney et al., 1985; Hönisch et al., 2013; Allen et al., 2015; Evans et al., 2015; Hauzer et al., 2018). The
418 insensitivity of shell K/Ca to seawater K/Ca most likely results either from a biological vital effect,
419 acting to increase the $[K^+]$ of the calcification site as $[Ca^{2+}]_{sw}$ increases to drive a much shallower
420 relationship between shell-seawater K/Ca than would otherwise be expected, or from a kinetic effect
421 on K incorporation into calcite driven by the differential $[Ca^{2+}]_{sw}$. We first briefly explore the former
422 possibility here, and the latter in more detail in Sec. 4.3.

423 Transmembrane alkali element pumps are ubiquitous (e.g. Nakao and Gadsby, 1986; Skou
424 and Esmann, 1992; Gouaux and MacKinnon, 2005). In foraminifera, proton pumping is known to
425 accompany calcification (Bentov et al., 2009; Toyofuku et al., 2017). Li-proton pumps have been
426 implicated in controlling the carbonate chemistry of the calcification site (Vigier et al., 2015), with Na-
427 proton pumps another likely candidate given the abundance of Na^+ in seawater (see e.g. Erez, 2003;
428 McNicholl et al., (2019)). Given that K^+ is present at a concentration of 10.2 mmol kg^{-1} in seawater and
429 at much higher concentrations in the cytosol of marine cells (>100 mM; Eppley, 1958; Dodd et al.,
430 1966; Thompson and MacLeod, 1974), the use of a K-proton pump as a means of regulating vacuole
431 or calcification site pH may be a likely possibility. At face value, the shallow slope resulting in elevated
432 K/Ca_{LBF} at higher $[Ca^{2+}]_{sw}$ would imply a greater degree of proton elevation and therefore a higher
433 $[K^+]$ at the calcification site in experiments with a higher-than-natural $[Ca^{2+}]_{sw}$. This may seem

unintuitive, given that at higher $[Ca^{2+}]_{sw}$, the saturation state of seawater (Ω_c) is higher, thus requiring a lower degree of pH elevation to achieve a similar degree of calcite precipitation. However, an alternative possibility is that a greater $[Ca^{2+}]_{sw}$ means that the organism can continue to precipitate calcite from the same package of seawater for longer, because more Ca^{2+} is available for calcification. If so, this continued precipitation would require a greater degree of proton pumping given that calcification releases protons, in order to maintain an elevated pH through this process to promote precipitation and CO_2 diffusion from the cytosol to the calcification site (as calcification is carbon limited in unmodified seawater). However, while calcification from seawater with an elevated $[Ca^{2+}]$ may well be associated with a greater degree of Li/Na/K pumping, as the organism makes use of the extra Ca^{2+} available, the high concentration of K^+ in seawater (K^+/H^+ = ~10^6) means that the calcification site $[K^+]$ is likely to be negligibly modified by this process (in contrast to Li; Vigier et al., 2015, we note that the same logic also applies to the calcification site $[Na^+]$). Thus, we argue that the highly nonlinear seawater-shell K/Ca relationship that we observe is perhaps more likely to represent a kinetic effect, driven by the control that $[Ca^{2+}]_{sw}$ has on the rate of mineral precipitation.

4.3. Evidence for a kinetic effect on K incorporation

The seawater $[Ca^{2+}]$ in the culture experiments utilised here was varied independently of all other parameters. As a result, the saturation state of these seawaters with respect to calcite (Ω_c) covaried with $[Ca^{2+}]_{sw}$, as $[CO_3^{2-}]$ remained constant. Because the carbonate chemistry of seawater is known to be an important control on both inorganic calcite precipitation and the calcification of foraminifera (e.g. Erez, 2003; Wolthers et al., 2012; Oron et al., 2020), it is possible that the experimental design could have affected not only the growth rate of the foraminifera (Hauzer et al., 2018), but also the crystal growth rates at the calcification site. Here, we explore whether this

phenomenon could explain the observed shallow slope of the relationship between seawater-shell K/Ca, i.e., if the elevated $[Ca^{2+}]_{sw}$ drove higher surface-area normalised crystal growth rates and therefore higher shell K/Ca for a given $[Ca^{2+}]_{sw}$ than would otherwise be expected if Ω_c had remained constant in these experiments.

In the culture experiment, population-scale calcification rate was calculated based on measurements of alkalinity depletion (Hauzer et al., 2018).. However, population-scale calcification rates may not necessarily represent crystal-precipitation rates for two reasons: i) not all foraminifera in our experiments calcified at the same rate. Because it is not practically feasible to weigh individual foraminifera to estimate the growth rate that is characteristic of the calcifying specimens (e.g. approximately 20% of foraminifera did not add any new chambers in culture), the overall calcification rate is biased downwards by specimens that did not grow in culture, and/or ii) irrespective of this complication, bulk calcification rate could be decoupled from surface area normalised precipitation rate at the calcification site because calcification is almost certainly a discontinuous process; chamber formation usually takes place at discrete intervals every few days. This is important because it is surface area-normalised precipitation rates that ultimately exert a large control on trace element incorporation into the growing mineral (Watson, 2004). To avoid these issues, and given that Ω_c and $[Ca^{2+}]_{sw}$ covaried in the culture experiment with varying Ca_{SW} (Fig. 5), we alternatively explore the extent to which Ω_c-driven crystal growth rate effect could impact our results by deriving an empirical relationship between Ω_c and K/Ca in *O. ammonoides* from the culture experiment in which *O. ammonoides* was grown at variable pH/Ω_c but constant DIC. In the supplementary materials we additionally formulate a theoretical relationship to account for the effect of variable $[Ca^{2+}]_{sw}$ on crystal growth rate and thus El/Ca_{LBF} (based on empirical growth rate equations and information from

478 inorganic precipitation experiments regarding the rate control on alkali element incorporation),
479 demonstrating that the direction of this effect is the same in both inorganic and foraminiferal calcite.
480 We stress that a precipitation rate-driven kinetic effect on K incorporation is not the only potential
481 explanation for the strong deviation of the data from a constant apparent distribution coefficient.
482 For example, differences in the degree of Ca utilization within the pool at the calcification site may
483 also be important (Elderfield et al., 1996), as may be large degrees of K^+ transport or leakage.
484 However, we focus on a kinetic effect here because our data demonstrate an impact of seawater
485 carbonate chemistry on foraminiferal K/Ca.

486 The results of this exercise are shown in Fig. 7. Here, a correction was applied to the seawater-
487 shell Na-K/Ca data using a relationship between shell El/Ca and Ω_c based on culture experiment at
488 varying pH (details in supplementary material). The results of this correction suggest that a
489 substantial portion of the apparent insensitivity of shell K/Ca to K/Ca_{sw} (Fig. 5) is mechanistically
490 explicable via a growth-rate driven kinetic control on K incorporation into calcite. Given that rate has
491 been shown to impact the incorporation of the alkali elements to a much greater degree than the
492 alkali earth elements in calcite (e.g. Lorens, 1981; Nehrke et al., 2007; Füger et al., 2019), Ω_c-driven
493 rate effect on K/Ca in our $[Ca^{2+}]_{sw}$ laboratory culture data should be accounted for before using these
494 results to understand the relationship between seawater and shell K/Ca. We note that even following
495 this correction, to our knowledge, the power relationship between seawater-shell K/Ca has a lower
496 power coefficient than any trace element studied so far, which could relate to a biological vital effect
497 (e.g. a higher $[K^+]$ of the calcification site driven by processes other than alkali-proton pumps), or
498 further kinetic effects (e.g. if the calcification site Ω_c is not characterised by a 1:1 relationship to
499 seawater Ω_c, when saturation state changes are driven by $[Ca^{2+}]_{sw}$.

In terms of using the laboratory culture calibration as a potential tool to reconstruct changes in $[Ca^{2+}]_{sw}$, we advocate for the use of the Ω_c-corrected equation (Fig 7). This is because Ω_c varied by 3.74 units in the seawater $[Ca^{2+}]_{sw}$ experiment, but is not thought to have undergone substantial variation in the (sub)tropical surface ocean through the Cenozoic (e.g. (Anagnostou et al., 2016; Tyrrell and Zeebe, 2004)). Therefore, if the notion that $[K^+]_{sw}$ was constant throughout the Cenozoic, as suggested by Horita et al., (2002) is correct, then the K/Ca calibration established in this study may be used for direct reconstruction of $[Ca^{2+}]_{sw}$.

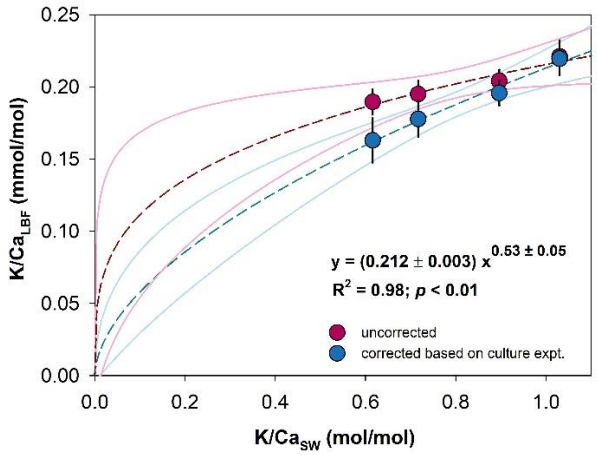

Fig. 7. The relationship between K/Ca_{LBF} and K/Ca_{sw}. A growth rate correction, explored here because $[Ca^{2+}]_{sw}$ in these culture experiments covaried with Ω_c is shown using the relationship between K/Ca and Ω_c from the experiment in which pH was varied at constant (modern) Ω_c. Error bars are 2SE. Solid lines depict the 95% confidence intervals of the least-squares power regressions. The equations given in the panels are those through the corrected K/Ca data.

4.4. Incorporation of K in $CaCO_3$

A better understanding of the processes by which marine carbonates incorporate trace elements from seawater is important in improving the accuracy of reconstructions based of shell geochemistry. Given that there is a limited amount of previous work on K incorporation in marine carbonates, we summarise most of the data published so far and place it in the context of inorganic

precipitation work in an attempt to identify the broad controls on K incorporation into biogenic $CaCO_3$.

Inorganic $CaCO_3$: Several studies have investigated the influence of various solution chemistry and physical parameters on alkali metal incorporation into calcite and aragonite. Ishikawa and Ichikuni (1984) examined the uptake of Na and K in inorganically precipitated calcite primarily as a function of solution $[Na^+]$ and $[K^+]$ and observed a clear control of solution El/Ca on their incorporation, demonstrating that both trace elements have a distribution coefficient in both $CaCO_3$ polymorphs. White (1977) investigated the mechanism of K incorporation in inorganically precipitated aragonite and observed that Na and K incorporation decreases with decreasing pH and increasing temperature, in addition to demonstrating an inhibition of K incorporation in the presence of high concentrations of Na, implying competition between these elements for certain sites or spaces within the lattice (although the range of solution alkali metal/Ca ratios investigated were far higher than those of our study). While we also observe a clear Na and K distribution coefficient (function) into biogenic high-Mg calcite, the overall much larger parameter space investigated in the inorganic experimental work conducted to-date likely explains why we do not observe many of these factors in marine biogenic $CaCO_3$.

Calcitic organisms: The nummulitid larger benthic foraminifer *Operculina* sp. analysed in the present study are formed of high-Mg calcite (Blackmon and Todd, 1959; Cotton et al., 2020). To the best of our knowledge, our data represent the first report of K/Ca in high-Mg calcite. These foraminifera have K/Ca = 0.21±0.100 (2SD) and $D_K = 2.2\times10^{-4}$ (averaged across all of our field and culture data) which is similar to the range of *G. ruber* reported here (0.23±0.097 (2SD); $D_K = 2.3\times10^{-4}$) and other low-Mg calcitic marine organisms (deep sea corals, brachiopods; (Li et al., (2021) Fig. 8)

with only the bivalves offset to significantly lower values. As such, there is no evidence for a mineralogical control on K incorporation, in contrast to Na and Sr, and possibly other trace elements (Evans et al., 2015; van Dijk et al., 2017). The *O. ammonoides* culture experiment presented here is the first time that the relationship between K/Ca_{shell} and K/Ca_{sw} has been assessed for a foraminifer species, demonstrating that K/Ca_{shell} is governed by K/Ca_{sw}, albeit with a shallow slope. Interestingly, this relationship is substantially shallower that those that have been described between Na/Ca_{shell} and Na/Ca_{sw} (Hauzer et al., 2018; Le Houedec et al., 2021; Zhou et al., 2021; Fig. 9). If the shallow slope of the seawater-shell K/Ca ratio in this experiment is indeed driven in part by kinetic processes (Sec. 4.3), this may imply a greater sensitivity of K incorporation to factors such as growth rate. Curiously, this is intuitively difficult to reconcile with the relative constancy between K/Ca across multiple groups of marine calcitic organisms, while the incorporation of other trace elements differs widely between these groups (Raja et al., 2007; Ulrich et al., 2021; Van Dijk et al., 2017); further work will be required to understand why this is the case. While it is beyond the scope of this study to investigate this in more detail, we note that the commonality of the power relationship between Na/Ca with Na/Ca_{sw} in all foraminifera studied so far, and a similar observation for K/Ca in biogenic calcite (Fig. 9a,b), suggests – at least – that the mechanism of Na and K incorporation may be similar in low-Mg planktic foraminifera and high-Mg large benthic foraminifera.

Aragonitic organisms: As is the case for the calcitic organisms, the K/Ca of a number of biogenic aragonites (corals, bivalves, gastropods) is characterised by a relatively narrow range (K/Ca: 0.20 to 0.25 mmol mol^{-1}), and absolute values that are indistinguishable from most biogenic calcites. This is in contrast to Na/Ca, which is a factor of ~2 higher in biogenic aragonite compared to biogenic low-Mg calcite (Schleinkofer et al., 2019). Thus, there is no evidence for a first-order mineralogical

control on K incorporation into $CaCO_3$, potentially implying that the calcification site K/Ca and K distribution coefficient may be similar across a large range of marine calcifying organisms, if shell K/Ca is alternatively primarily determined by K/Ca_{sw}. A review of the limited amount of existing research indicates that this assumption of a primary K/Ca_{sw} control is the case for some aragonitic organisms but not others. K/Ca measured in the aragonitic shells of gastropods showed no relationship with fluid K/Ca (Rosenthal and Katz, 1989), although this study reported data for a freshwater species. In contrast, K/Ca and Na/Ca of aragonitic scleractinian corals follow a near linear relationship with El/Ca_{sw} (Ram and Erez, 2021), which has similarly been shown to be the case for inorganically precipitated K/Ca and Na/Ca (at least up to seawater-like K-Na/Ca ratios; Okumura and Kitano, 1986).

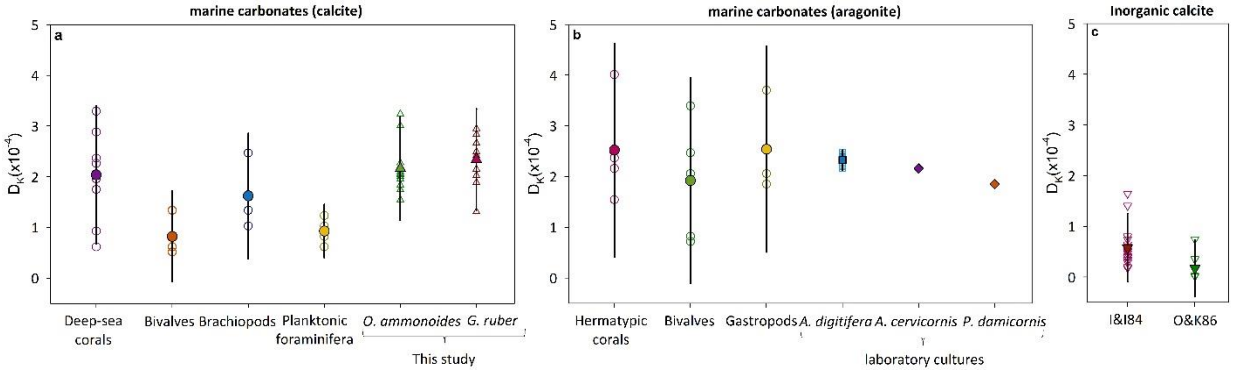

Fig. 8. The D_K in a) calcitic biogenic marine carbonates, b) aragonitic marine carbonates and c) inorganic calcite. The D_K estimations are based on solution K and Ca concentrations, except in the case of the inorganic calcite study of I&I84, in which the D_K values are based on K activity. The symbols denote: this study (triangles; open triangles indicate specimens from different locations and culture study), Li et al., 2021 (circle; open circles indicate different species); Bell et al., 2018 (square; open squares indicate different specimens); Ram and Erez, 2021 (diamond) and inverted triangles (I&I84: Ishikawa and Ichikuni, 1984; O&K,86: Okumura and Kitano, 1986). Solid symbols are average values. In all cases error bars denote the 2SD of each dataset, but note that each dataset represents a wide range of sample collection types (multiple/single species, culture/natural populations etc., see brackets in the earlier part of the figure caption for brief descriptions).

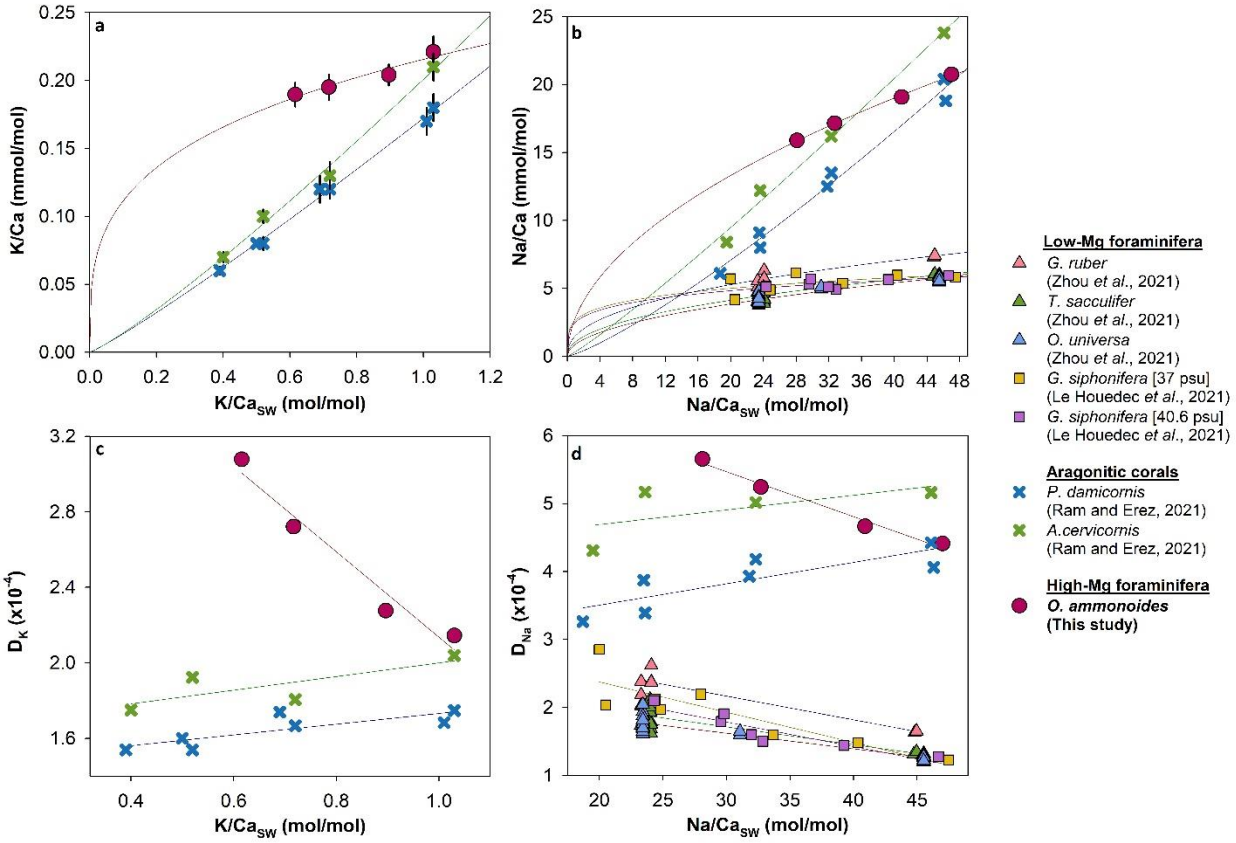

Fig. 9. a,b) The relationship between K/Ca and Na/Ca of different marine carbonates and El/Ca$_{sw}$. c,d) The relationship between the apparent distribution coefficient of K (D_K) and Na (D_{Na}) with their El/Ca$_{sw}$. All error bars are 2SE.

Both our work and a previous study (Ram and Erez, 2021) demonstrate that the partition of K in marine carbonates is governed to large degree by the K/Ca$_{sw}$ ratio. The apparent distribution coefficient of K in *O. ammonoides*, calculated as $D_{El} = (El/Ca)_{shell}/(El/Ca)_{sw}$, decreases with increasing K/Ca$_{sw}$, a behaviour which is similar to that of Na (Fig. 9c,d) and Mg in a wide range of biogenic calcites (Hasiuk and Lohmann, 2010) and inorganic calcite (Mucci and Morse, 1983). To facilitate the comparison of K and Na distribution coefficients presented here to other marine carbonates, we compile apparent distribution coefficient data as a function of the respective seawater ratio (Fig. 9c,d). The D_{Na} of both planktonic foraminifera and larger benthic foraminifera showed a decreasing trend with increasing seawater Na/Ca, whereas the D_K and D_{Na} of two aragonitic scleractinian corals

595 is characterised by a shallow positive slope with El/Ca_{sw} (Ram and Erez, 2021). As we discuss above,
596 this is perhaps most parsimoniously explained by a kinetic (growth rate) effect on the incorporation
597 of K and Na in the foraminifera which results in higher D_{El} with increasing Ca_{sw}, although we again
598 note that understanding the degree of Rayleigh fractionation at the calcification site of calcifying
599 organisms is also key in terms of understanding bulk calcite trace element geochemistry (Elderfield
600 et al., 1996; Evans et al., 2018b). Culture experiments that vary $[K^+]_{sw}$ rather than $[Ca^{2+}]_{sw}$ would be
601 one way in which this hypothesis could be tested. In addition, inorganic precipitation experiments
602 focusing on both calcite and aragonite are required to understand why this affect does not seem to
603 have biased the coral data, given that the foraminifera $[Ca^{2+}]_{sw}$ experiment discussed here was
604 experimentally similar to that of Ram and Erez, (2021).

605 **5. Summary**

606 In this study, we investigated the influence of a wide range of seawater parameters on the
607 incorporation of K into the planktonic foraminifer, *Globigerinoides ruber* (white) and larger benthic
608 foraminifer, *Operculina* sp.. In both cases, no significant correlation of K/Ca with temperature, salinity,
609 pH, or $[CO_3^{2-}]$ was observed, which suggests that the incorporation of K is independent of these
610 seawater parameters, or that other factors act to easily mask these effects. The similar K/Ca of low-
611 Mg planktonic foraminifera and high-Mg benthic foraminifera suggest no major effect of mineralogy
612 on K incorporation, which also appears to be more broadly the case (i.e. between calcite and
613 aragonite) based on a compilation of published data.

614 In addition, we investigated K/Ca in marine carbonate as a potential proxy for the seawater
615 K/Ca ratio, based on laboratory cultures of *Operculina ammonoides*. Given that previous work has
616 suggested that large changes in $[K^+]_{sw}$ have not occurred (Horita et al., 2002), this may be an

617 additional tool for understanding past changes in $[Ca^{2+}]_{sw}$. We show that a power relationship best
618 describes seawater-shell K/Ca, implying a variable apparent distribution coefficient. Indeed, the slope
619 of the K/Ca - K/Ca_{sw} relationship is very shallow, indicating another major control on K incorporation
620 into foraminifera. We suggest that this shallow relationship is, at least in part, the result of a kinetic
621 growth rate effect on K incorporation in *O. ammonoides* cultured at elevated $[Ca^{2+}]_{sw}$, although
622 further work will be required to conclusively rule out other possibilities such as K transport into the
623 calcifying fluid. The mechanistic basis of this could be that in the laboratory culture experiment
624 reported here, $[Ca^{2+}]_{sw}$ was varied in isolation, which means that $[Ca^{2+}]_{sw}$ and the saturation state of
625 seawater (Ω_c) covaried. Because Ω_c is one of the dominant controls on surface area-normalised
626 precipitation rate, we propose that a crystal growth rate effect may explain the shallow seawater-
627 shell K/Ca relationship, driving K/Ca to higher ratios at elevated $[Ca^{2+}]_{sw}$. We corrected for this using
628 a relationship between Ω_c and K/Ca derived from a second culture experiment in which *O.*
629 *ammonoides* was grown at different seawater pH values, which has the effect of increasing the slope
630 of the seawater-shell K/Ca relationship. Given that surface ocean Ω_c has likely not varied to a large
631 degree over the Cenozoic (e.g. Tyrrell and Zeebe, 2004; Ridgwell and Zeebe, 2005), we argue that
632 this corrected relationship should be applied in the geologic past, and that the slope of this curve is
633 sufficiently steep to make K/Ca a potentially useful tool for unravelling past changes in seawater
634 major ion chemistry. Given that other seawater parameters show no resolvable influence on K
635 incorporation into foraminifera, and if the notion that the seawater $[K^+]$ has remained constant
636 through the Phanerozoic Eon is correct (Horita et al., 2002), this calibration could therefore be used
637 as a tool to reconstruct $[Ca^{2+}]_{sw.}$ Ultimately, combining Na/Ca (Hauzer et al., 2018; Zhou et al., 2021)
638 and K/Ca data from the same specimens may be a potential means of further improving the accuracy

of reconstructions of the history of seawater [Ca^{2+}] variability, or could be used to determine whether seawater [Na^{+}] and [K^{+}] have indeed remained within narrow bounds. Because *O. ammonoides* are a close relative of the nummulitid foraminifera which were abundant during the Paleogene (Hallock, 1985; Holzmann et al., 2003), this group, and the calibration presented here, may represent a good target for the reconstruction of Cenozoic seawater chemistry, opening up new possibilities in terms of understanding the processes that govern the seawater Ca cycle.

Acknowledgments

This work is part of the VeWA consortium funded by the Hessen State Ministry for Higher Education, Research, and the Arts through the LOEWE program. MJH gratefully acknowledges the provision of sample materials by Michal Kucera and Helen Bostock. The foraminifera culture work of HH and DE was carried out in the laboratory of J.Erez and funded by ISF grant # 1886/20. FIERCE is financially supported by the Wilhelm and Else Heraeus Foundation and by the Deutsche Forschungsgemeinschaft (DFG: INST 161/921-1 FUGG, INST 161/923-1 FUGG and INST 161/1073-1 FUGG), which is gratefully acknowledged. This is FIERCE contribution No. 126. We gratefully thank the associate editor Tom Marchitto, as well as Sambuddha Misra and an anonymous reviewer for their thoughtful consideration of this work.

Appendix A. Supplementary material

The supplementary table contains detail information on the analytical setup, analytical performance, the El/Ca data of all foraminifera from modern seawater, and the culture experiments investigated in this study. The supplementary PDF file includes further discussion on the analytical performance, carbonate chemistry culture experiment, and the growth rate correction of the K/Ca_{LBF}-K/Ca_{sw} relationship.

References

Allen, K.A., Hönisch, B., 2012. The planktic foraminiferal B/Ca proxy for seawater carbonate chemistry: A critical evaluation. Earth Planet. Sci. Lett. 345, 203–211.

Allen, K.A., Hönisch, B., Eggins, S.M., Haynes, L.L., Rosenthal, Y., Yu, J., 2016. Trace element proxies for surface ocean conditions: A synthesis of culture calibrations with planktic foraminifera. Geochim. Cosmochim. Acta 193, 197–221.

Anagnostou, E., John, E.H., Edgar, K.M., Foster, G.L., Ridgwell, A., Inglis, G.N., Pancost, R.D., Lunt, D.J., Pearson, P.N., 2016. Changing atmospheric CO2 concentration was the primary driver of early Cenozoic climate. Nature 533, 380–384.

671 Anand, P., Elderfield, H., Conte, M.H., 2003. Calibration of Mg/Ca thermometry in planktonic
672 foraminifera from a sediment trap time series. Paleoceanography 18, 2.

673 Bell, T., Iguchi, A., Suzuki, A., Seki, A., Yokoyama, Y., 2018. Testing possible relationships between
674 Acropora digitifera genes, seawater chemistry and skeletal elements. Geochem. J. 52, 263–272.

675 Bentov, S., Brownlee, C., Erez, J., 2009. The role of seawater endocytosis in the biomineralization
676 process in calcareous foraminifera. Proc. Natl. Acad. Sci. U.S.A. 106, 21500–21504.

677 Bertlich, J., Nürnberg, D., Hathorne, E.C., De Nooijer, L.J., Mezger, E.M., Kienast, M., Nordhausen, S.,
678 Reichart, G.J., Schönfeld, J., Bijma, J., 2018. Salinity control on Na incorporation into calcite tests
679 of the planktonic foraminifera Trilobatus sacculifer - Evidence from culture experiments and
680 surface sediments. Biogeosciences 15, 5991–6018.

681 Blackmon, P.D., Todd, R., 1959. Mineralogy of some foraminifera as related to their classification and
682 ecology. J. Paleontol. 1–15.

683 Bloch, S., Bischoff, J.L., 1979. The effect of low-temperature alteration of basalt on the oceanic budget
684 of potassium. Geology 7, 193–196.

685 Bonnin, E.A., Zhu, Z., Fehrenbacher, J.S., Russell, A.D., Hönisch, B., Spero, H.J., Gagnon, A.C., 2019.
686 Submicron sodium banding in cultured planktic foraminifera shells. Geochim. Cosmochim. Acta
687 253, 127–141.

688 Boyle, E.A., 1981. Cadmium, zinc, copper, and barium in foraminifera tests. Earth Planet. Sci. Lett. 53,
689 11–35.

690 Branson, O., Bonnin, E.A., Perea, D.E., Spero, H.J., Zhu, Z., Winters, M., Hönisch, B., Russell, A.D.,
691 Fehrenbacher, J.S., Gagnon, A.C., 2016. Nanometer-scale chemistry of a calcite biomineralization
692 template: Implications for skeletal composition and nucleation. PNAS 113, 12934–12939.

693 Broecker, W.S., Peng, T.H., 1982. Tracers in the Sea, Lamont-Doherty geological observatory.
694 Palisades, New York.

695 Brown, R.E., Anderson, L.D., Thomas, E., Zachos, J.C., 2011. A core-top calibration of B/Ca in the
696 benthic foraminifers Nuttallides umbonifera and Oridorsalis umbonatus: A proxy for Cenozoic
697 bottom water carbonate saturation. Earth Planet. Sci. Lett. 310, 360–368.

698 Carpenter, W.B., 1862. Introduction to the Study of the Foraminifera: By William B. Carpenter, Assisted
699 by William K. Parker and T. Rupert Jones. Publ. for the Ray Society, Hardwicke.

700 Coggon, R.M., Teagle, D.A.H., Smith-Duque, C.E., Alt, J.C., Cooper, M.J., 2010. Reconstructing past
701 seawater Mg/Ca and Sr/Ca from mid-ocean ridge flank calcium carbonate veins. Science 327,
702 1114–1117.

703 Coogan, L.A., Dosso, S.E., 2015. Alteration of ocean crust provides a strong temperature dependent
704 feedback on the geological carbon cycle and is a primary driver of the Sr-isotopic composition
705 of seawater. Earth Planet. Sci. Lett. 415, 38–46.

706 Cotton, L. J., Evans, D., & Beavington-Penney, S. J., 2020. The high-magnesium calcite origin of

707 nummulitid foraminifera and implications for the identification of calcite diagenesis. Palaios 35,
708 421-431.

709 De Nooijer, L.J., Toyofuku, T., Kitazato, H., 2009. Foraminifera promote calcification by elevating their
710 intracellular pH. PNAS 106, 15374–15378.

711 Delaney, M.L., Bé, A.W.H., Boyle, E.A., 1985. Li, Sr, Mg, and Na in foraminiferal calcite shells from
712 laboratory culture, sediment traps, and sediment cores. Geochim. Cosmochim. Acta 49, 1327–
713 1341.

714 Delaney, M.L., Popp, B.N., Lepzelter, C.G., Anderson, T.F., 1989. Lithium-to-calcium ratios in Modern,
715 Cenozoic, and Paleozoic articulate brachiopod shells. Paleoceanography 4, 681–691.

716 Dickson, A.G., Wesolowski, D.J., Palmer, D.A., Mesmer, R.E., 1990. Dissociation constant of bisulfate
717 ion in aqueous sodium chloride solutions to 250 °C. J. Phys. Chem. 94, 7978–7985.

718 Dickson, J.A.D., 2002. Fossil echinoderms as monitor of the Mg/Ca ratio of Phanerozoic oceans.
719 Science 298, 1222–1224.

720 Dodd, W., Pitman, M., West, K., 1966. Sodium and potassium transport in the marine alga
721 Chaetomorpha darwinii. Aust. J. Biol. Sci. 19, 341.

722 Dunlea, A.G., Murray, R.W., Santiago Ramos, D.P., Higgins, J.A., 2017. Cenozoic global cooling and
723 increased seawater Mg/Ca via reduced reverse weathering. Nat. Commun. 8, 1–6.

724 Elderfield, H., Bertram, C.J., Erez, J., 1996. A biomineralization model for the incorporation of trace
725 elements into foraminiferal calcium carbonate. Earth Planet. Sci. Lett. 142, 409–423.

726 Eppley, R.W., 1958. Sodium exclusion and potassium retention by the red marine alga, Porphyra
727 perforata. J. Gen. Physiol. 41, 901.

728 Erez, J., 2003. The source of ions for biomineralization in foraminifera and their implications for
729 paleoceanographic proxies. Rev. Mineral. Geochem. 54, 115–149.

730 Evans, D., Badger, M.P.S., Foster, G.L., Henehan, M.J., Lear, C.H., Zachos, J.C., 2018a. No substantial
731 long-term bias in the Cenozoic benthic foraminifera oxygen-isotope record. Nat. Commun. 9,
732 17–19.

733 Evans, D., Erez, J., Oron, S., Müller, W., 2015. Mg/Ca-temperature and seawater-test chemistry
734 relationships in the shallow-dwelling large benthic foraminifera Operculina ammonoides.
735 Geochim. Cosmochim. Acta 148, 325–342.

736 Evans, D., Müller, W., 2018. Automated extraction of a five-year LA-ICP-MS trace element data set of
737 ten common glass and carbonate reference materials: Long-term data quality, optimisation and
738 laser cell homogeneity. Geostand. Geoanal. Res 2,159-188.

739 Evans, D., Müller, W., 2013. LA-ICPMS elemental imaging of complex discontinuous carbonates: An
740 example using large benthic foraminifera. J. Anal. At. Spectrom. 28, 1039–1044.

741 Evans, D., Müller, W., 2012. Deep time foraminifera Mg/Ca paleothermometry: Nonlinear correction
742 for secular change in seawater Mg/Ca. Paleoceanography 27, 4.

743 Evans, D., Müller, W., Erez, J., 2018b. Assessing foraminifera biomineralisation models through trace
744 element data of cultures under variable seawater chemistry. Geochim. Cosmochim. Acta 236,
745 198–217.

746 Evans, D., Müller, W., Oron, S., Renema, W., 2013. Eocene seasonality and seawater alkaline earth
747 reconstruction using shallow-dwelling large benthic foraminifera. Earth Planet. Sci. Lett. 381,
748 104–115.

749 Evans, D., Wade, B.S., Henehan, M., Erez, J., Müller, W., 2016. Revisiting carbonate chemistry controls
750 on planktic foraminifera Mg/Ca: Implications for sea surface temperature and hydrology shifts
751 over the Paleocene-Eocene Thermal Maximum and Eocene-Oligocene transition. Clim. Past 12,
752 819–835.

753 Füger, A., Konrad, F., Leis, A., Dietzel, M., Mavromatis, V., 2019. Effect of growth rate and pH on
754 lithium incorporation in calcite. Geochim. Cosmochim. Acta 248, 14–24.

755 Garbe-Schönberg, D., Müller, S., 2014. Nano-particulate pressed powder tablets for LA-ICP-MS. J.
756 Anal. At. Spectrom. 29, 990–1000.

757 Geerken, E., de Nooijer, L.J., Roepert, A., Polerecky, L., King, H.E., Reichart, G.J., 2019. Element banding
758 and organic linings within chamber walls of two benthic foraminifera. Sci. Rep. 9, 1–15.

759 Gothmann, A.M., Stolarski, J., Adkins, J.F., Schoene, B., Dennis, K.J., Schrag, D.P., Mazur, M., Bender,
760 M.L., 2015. Fossil corals as an archive of secular variations in seawater chemistry since the
761 Mesozoic. Geochim. Cosmochim. Acta 160, 188–208.

762 Gouaux, E., MacKinnon, R., 2005. Principles of selective ion transport in channels and pumps. Science
763 310, 1461–1465.

764 Gray, W.R., Evans, D., 2019. Nonthermal influences on Mg/Ca in planktonic foraminifera: A review of
765 culture studies and application to the last glacial maximum. Paleoceanogr. Paleoclimatol. 34,
766 306–315.

767 Gray, W.R., Weldeab, S., Lea, D.W., Rosenthal, Y., Gruber, N., Donner, B., Fischer, G., 2018. The effects
768 of temperature, salinity, and the carbonate system on Mg/Ca in Globigerinoides ruber (white):
769 A global sediment trap calibration. Earth Planet. Sci. Lett. 482, 607–620.

770 Gregor, L., Gruber, N., 2021. OceanSODA-ETHZ: A global gridded data set of the surface ocean
771 carbonate system for seasonal to decadal studies of ocean acidification. Earth Syst. Sci. Data 13,
772 777–808.

773 Hallock, P., 1985. Why are larger foraminifera large? Paleobiology 11, 195–208.

774 Hardie, L.A., 1996. Secular variation in seawater chemistry: An explanation for the coupled secular
775 variation in the mineralogies of marine limestones and potash evaporites over the past 600 m.y.
776 Geology 24, 279–283.

777 Hasiuk, F.J., Lohmann, K.C., 2010. Application of calcite Mg partitioning functions to the
778 reconstruction of paleocean Mg/Ca. Geochim. Cosmochim. Acta 74, 6751–6763.

779 Hauzer, H., 2022. Development of new foraminiferal proxies for paleochemistry of the oceans. PhD
780 thesis. the Hebrew University of Jerusalem.

781 Hauzer, H., Evans, D., Müller, W., Rosenthal, Y., Erez, J., 2021. Salinity effect on trace element
782 incorporation in cultured shells of the large benthic foraminifer Operculina ammonoides.
783 Paleoceanogr. Paleoclimatol. 36, 1–19.

784 Hauzer, H., Evans, D., Müller, W., Rosenthal, Y., Erez, J., 2018. Calibration of Na partitioning in the
785 calcitic foraminifer Operculina ammonoides under variable Ca concentration: Toward
786 reconstructing past seawater composition. Earth Planet. Sci. Lett. 497, 80–91.

787 Heinrich, C.A., Pettke, T., Halter, W.E., Aigner-Torres, M., Audétat, A., Günther, D., Hattendorf, B.,
788 Bleiner, D., Guillong, M., Horn, I., 2003. Quantitative multi-element analysis of minerals, fluid
789 and melt inclusions by laser-ablation inductively-coupled-plasma mass-spectrometry. Geochim.
790 Cosmochim. Acta 67, 3473–3497.

791 Henehan, M.J., Foster, G.L., Rae, J.W.B., Prentice, K.C., Erez, J., Bostock, H.C., Marshall, B.J., Wilson,
792 P.A., 2015. Evaluating the utility of B/Ca ratios in planktic foraminifera as a proxy for the
793 carbonate system: A case study of Globigerinoides ruber. Geochem. Geophys. Geosyst. 16,
794 1052–1069.

795 Higgins, J.A., Schrag, D.P., 2015. The Mg isotopic composition of Cenozoic seawater - evidence for a
796 link between Mg-clays, seawater Mg/Ca, and climate. Earth Planet. Sci. Lett. 416, 73–81.

797 Hohenegger, J., 2011. Large foraminifera: greenhouse constructions and gardeners in the oceanic
798 microcosm. The Kagoshima University Museum, Kagoshima, Japan.

799 Holzmann, M., Hohenegger, J., Pawlowski, jan, 2003. Molecular data reveal parallel evolution in
800 nummulitid foraminifera. J. Foraminiferal Res. 33, 277–284.

801 Horita, J., Zimmermann, H., Holland, H.D., 2002. Chemical evolution of seawater during the
802 Phanerozoic: Implications from the record of marine evaporites. Geochim. Cosmochim. Acta 66,
803 3733–3756.

804 Ishikawa, M., Ichikuni, M., 1984. Uptake of sodium and potassium by calcite. Chem. Geol. 42, 137–146.

805 Isson, T.T., Planavsky, N.J., 2018. Reverse weathering as a long-term stabilizer of marine pH and
806 planetary climate. Nature 560, 471–475.

807 Jochum, K.P., Garbe-Schönberg, D., Veter, M., Stoll, B., Weis, U., Weber, M., Lugli, F., Jentzen, A.,
808 Schiebel, R., Wassenburg, J.A., others, 2019. Nano-powdered calcium carbonate reference
809 materials: Significant progress for microanalysis? Geostand. Geoanal. Res. 43, 595–609.

810 Jochum, K.P., Stoll, B., Herwig, K., Willbold, M., Hofmiann, A.W., Amini, M., Aarburg, S., Abouchami,
811 W., Hellebrand, E., Mocek, B., Raczek, I., Stracke, A., Alard, O., Bouman, C., Becker, S., Dücking,
812 M., Brätz, H., Klemd, R., De Bruin, D., Canil, D., Cornell, D., De Hoog, C.J., Dalpé, C.,
813 Danyushevshy, L., Eisenhauer, A., Gao, Y., Snow, J.E., Groschopf, N., Günther, D., Latkoczy, C.,
814 Guillong, M., Hauri, E.H., Höfer, H.E., Lahaye, Y., Horz, K., Jacob, D.E., Kasemann, S.A., Kent, A.J.R.,
815 Ludwig, T., Zack, T., Mason, P.R.D., Meixner, A., Rosner, M., Misawa, K., Nash, B.P., Pfänder, J.,

Premo, W.R., Sun, W.D., Tiepolo, M., Vannucci, R., Vennemann, T., Wayne, D., Woodhead, J.D., 2006. MPI-DING reference glasses for in situ microanalysis: New reference values for element concentrations and isotope ratios. Geochem. Geophys. Geosyst. 7.

Jochum, K.P., Weis, U., Stoll, B., Kuzmin, D., Yang, Q., Raczek, I., Jacob, D.E., Stracke, A., Birbaum, K., Frick, D. a., Günther, D., Enzweiler, J., 2011. Determination of Reference Values for NIST SRM 610-617 Glasses Following ISO Guidelines. Geostand. Geoanal. Res. 35, 397-429.

Keul, N., Langer, G., De Nooijer, L.J., Bijma, J., 2013. Effect of ocean acidification on the benthic foraminifera Ammonia sp. is caused by a decrease in carbonate ion concentration. Biogeosciences 10, 6185–6198.

Kronberg, B.I., 1985. Weathering dynamics and geosphere mixing with reference to the potassium cycle. Phys. Earth Planet. Inter 41, 125–132.

Le Houedec, S., Erez, J., Rosenthal, Y., 2021. Testing the influence of changing seawater Ca concentration on elements/Ca ratios in planktic foraminifera: A culture experiment. Geochem. Geophys. Geosyst. 22, 3.

Lea, D.W., Mashiotta, T.A., Spero, H.J., 1999. Controls on magnesium and strontium uptake in planktonic foraminifera determined by live culturing. Geochim. Cosmochim. Acta 63, 2369–2379.

Lee, K., Kim, T.-W., Byrne, R.H., Millero, F.J., Feely, R.A., Liu, Y.-M., 2010. The universal ratio of boron to chlorinity for the North Pacific and North Atlantic oceans. Geochim. Cosmochim. Acta 74, 1801–1811.

Li, W., Liu, X.M., Wang, K., Fodrie, F.J., Yoshimura, T., Hu, Y.F., 2021. Potassium phases and isotopic composition in modern marine biogenic carbonates. Geochim. Cosmochim. Acta 304, 364–380.

Locarnini, M., Mishonov, A. V, Baranova, O.K., Boyer, T.P., Zweng, M.M., Garcia, H.E., Seidov, D., Weathers, K., Paver, C., Smolyar, I., others, 2018. World ocean atlas 2018, volume 1: Temperature.

Lorens, R.B., 1981. Sr, Cd, Mn and Co distribution coefficients in calcite as a function of calcite precipitation rate. Geochim. Cosmochim. Acta 45, 553–561.

Lowenstein, T.K., Kendall, B., Anbar, A.D., 2014. The Geologic History of Seawater, Treatise on Geochemistry: Second Edition. Lowenstein, T.K., Timofeeff, M.N., Brennan, S.T., Hardie, L.A., Demicco, R. V., 2001. Oscillations in Phanerozoic seawater chemistry: Evidence from fluid Inclusions. Science 294, 1086–1088.

Lueker, T.J., Dickson, A.G., Keeling, C.D., 2000. Ocean pCO2 calculated from dissolved inorganic carbon, alkalinity, and equations for K1 and K2: validation based on laboratory measurements of CO2 in gas and seawater at equilibrium. Mar. Chem. 70, 105–119.

Marchitto Jr, T.M., Curry, W.B., Oppo, D.W., 2000. Zinc concentrations in benthic foraminifera reflect seawater chemistry. Paleoceanography 15, 299–306.

Marchitto, T.M., Bryan, S.P., Doss, W., McCulloch, M.T., Montagna, P., 2018. A simple biomineralization model to explain Li, Mg, and Sr incorporation into aragonitic foraminifera and corals. Earth

853 Planet. Sci. Lett. 481, 20–29.

854 Marriott, C.S., Henderson, G.M., Belshaw, N.S., Tudhope, A.W., 2004. Temperature dependence of
855 δ7Li, δ44Ca and Li/Ca during growth of calcium carbonate. Earth Planet. Sci. Lett. 222, 615–624.

856 McCauley, S.E., DePaolo, D.J., 1997. The marine 87Sr/86Sr and δ18O records, Himalayan alkalinity
857 fluxes, and Cenozoic climate models. Tectonic uplift and climate change 427–467.

858 McNicholl, C., Koch, M.S., Hofmann, L.C., 2019. Photosynthesis and light-dependent proton pumps
859 increase boundary layer pH in tropical macroalgae: A proposed mechanism to sustain
860 calcification under ocean acidification. J. Exp. Mar. Biol. Ecol. 521, 151208.

861 Mezger, E.M., de Nooijer, L.J., Boer, W., Brummer, G.J.A., Reichart, G.J., 2016. Salinity controls on Na
862 incorporation in Red Sea planktonic foraminifera. Paleoceanography 31, 1562–1582.

863 Michalopoulos, P., Aller, R.C., 1995. Rapid clay mineral formation in Amazon delta sediments: Reverse
864 weathering and oceanic elemental cycles. Science 270, 614–617.

865 Misra, S., Froelich, P.N., 2012. Lithium isotope history of cenozoic seawater: Changes in silicate
866 weathering and reverse weathering. Science 335, 818–823.

867 Mucci, A., Morse, J.W., 1984. The solubility of calcite in seawater solutions of various magnesium
868 concentration, It = 0.697m at 25 °C and one atmosphere total pressure. Geochim. Cosmochim.
869 Acta 48, 815–822.

870 Mucci, A., Morse, J.W., 1983. The incorporation of Mg2+ and Sr2+ into calcite overgrowths: influences
871 of growth rate and solution composition. Geochim. Cosmochim. Acta 47, 217–233.

872 Müller, W., Shelley, M., Miller, P., Broude, S., 2009. Initial performance metrics of a new custom-
873 designed ArF excimer LA-ICPMS system coupled to a two-volume laser-ablation cell. J. Anal.
874 At. Spectrom. 24, 209–214.

875 Nakao, M., Gadsby, D.C., 1986. Voltage dependence of Na translocation by the Na/K pump. Nature
876 323, 628–630.

877 Nehrke, G., Reichart, G.J., Van Cappellen, P., Meile, C., Bijma, J., 2007. Dependence of calcite growth
878 rate and Sr partitioning on solution stoichiometry: Non-Kossel crystal growth. Geochim.
879 Cosmochim. Acta 71, 2240–2249.

880 Okai, T., Suzuki, A., Kawahata, H., Terashima, S., Imai, N., 2002. Preparation of a new Geological
881 Survey of Japan geochemical reference material: Coral JCp-1. Geostand. newsl. 26, 95–99.

882 Okumura, M., Kitano, Y., 1986. Coprecipitation of alkali metal ions with calcium carbonate. Geochim.
883 Cosmochim. Acta 50, 49–58.

884 Oron, S., Evans, D., Abramovich, S., Almogi-Labin, A., Erez, J., 2020. Differential Sensitivity of a
885 Symbiont-Bearing Foraminifer to Seawater Carbonate Chemistry in a Decoupled DIC-pH
886 Experiment. Journal of Geophysical Research: Biogeosciences 125, 1–16.

887 Pearce, N.J.G., Perkins, W.T., Westgate, J.A., Gorton, M.P., Jackson, S.E., Neal, C.R., Chenery, S.P., 1997.
888 A compilation of new and published major and trace element data for NIST SRM 610 and NIST

SRM 612 glass reference materials. Geostand. newsl. 21, 115–144.

Pierrot, D., Epitalon, J.-M., Orr, J.C., Lewis, E., Wallace, D.W.R., 2021. MS Excel program developed for CO2 system calculations–version 3.0.

Raja, R., Saraswati, P.K., Iwao, K., 2007. A field-based study on variation in Mg/Ca and Sr/Ca in larger benthic foraminifera. Geochem. Geophys. Geosyst. 8, 10.

Ram, S., Erez, J., 2021. The Distribution Coefficients of Major and Minor Elements in Coral Skeletons Under Variable Calcium Seawater Concentrations. Front. Earth Sci. 9, 1–14.

Raymo, M.E., Ruddiman, W.F., 1992. Tectonic forcing of late Cenozoic climate. Nature 359, 117–122.

Renema, W., 2008. Habitat selective factors influencing the distribution of larger benthic foraminiferal assemblages over the Kepulauan Seribu. Mar. Micropaleontol. 68, 286–298.

Renema, W., 2006. Habitat variables determining the occurrence of large benthic foraminifera in the Berau area (East Kalimantan, Indonesia). Coral Reefs 25, 351–359.

Rickaby, R.E.M., Elderfield, H., 1999. Planktonic foraminiferal Cd/Ca: paleonutrients or paleotemperature? Paleoceanography 14, 293–303.

Ridgwell, A., Zeebe, R.E., 2005. The role of the global carbonate cycle in the regulation and evolution of the Earth system. Earth Planet. Sci. Lett. 234, 299–315.

Roberts, J., Kaczmarek, K., Langer, G., Skinner, L.C., Bijma, J., Bradbury, H., Turchyn, A. V, Lamy, F., Misra, S., 2018. Lithium isotopic composition of benthic foraminifera: A new proxy for paleo-pH reconstruction. Geochim. Cosmochim. Acta 236, 336–350.

Rosenthal, Y., Boyle, E.A., Slowey, N., 1997. Temperature control on the incorporation of magnesium, strontium, fluorine, and cadmium into benthic foraminiferal shells from Little Bahama Bank: Prospects for thermocline paleoceanography. Geochim. Cosmochim. Acta 61, 3633–3643.

Rosenthal, Y., Katz, A., 1989. The applicability of trace elements in freshwater shells for paleogeochemical studies. Chem. Geol. 78, 65–76.

Schleinkofer, N., Raddatz, J., Freiwald, A., Evans, D., Beuck, L., Rüggeberg, A., Liebetrau, V., 2019. Environmental and biological controls on Na/Ca ratios in scleractinian cold-water corals. Biogeosciences 16, 3565–3582.

Segev, E., Erez, J., 2006. Effect of Mg/Ca ratio in seawater on shell composition in shallow benthic foraminifera. Geochem. Geophys. Geosyst. 7, 1–8.

Skou, J.C., Esmann, M., 1992. The Na,K-ATPase. J. Bioenerg. Biomembr. 24, 249–261.

Thompson, J., MacLeod, R.A., 1974. Potassium transport and the relationship between intracellular potassium concentration and amino acid uptake by cells of a marine pseudomonad. J. Bacteriol. 120, 598–603.

Toyofuku, T., Matsuo, M.Y., De Nooijer, L.J., Nagai, Y., Kawada, S., Fujita, K., Reichart, G.J., Nomaki, H., Tsuchiya, M., Sakaguchi, H., Kitazato, H., 2017. Proton pumping accompanies calcification in

foraminifera. Nat. Commun. 8, 6–11.

Turchyn, A. V, DePaolo, D.J., 2019. Seawater chemistry through Phanerozoic time. Annu. Rev. Earth Planet. Sci 47, 197–224.

Tyrrell, T., Zeebe, R.E., 2004. History of carbonate ion concentration over the last 100 million years. Geochim. Cosmochim. Acta 68, 3521–3530.

Ulrich, R.N., Guillermic, M., Campbell, J., Hakim, A., Han, R., Singh, S., Stewart, J.D., Román-Palacios, C., Carroll, H.M., De Corte, I., Gilmore, R.E., Doss, W., Tripati, A., Ries, J.B., Eagle, R.A., 2021. Patterns of element incorporation in calcium carbonate biominerals recapitulate phylogeny for a diverse range of marine calcifiers. Front. Earth Sci. 9, 1–26.

van Dijk, I., de Nooijer, L.J., Wolthers, M., Reichart, G.J., 2017. Impacts of pH and [CO32-] on the incorporation of Zn in foraminiferal calcite. Geochim. Cosmochim. Acta 197, 263–277.

Van Dijk, I., Nooijer De, L.J., Reichart, G.J., 2017. Trends in element incorporation in hyaline and porcelaneous foraminifera as a function of pCO2. Biogeosciences 14, 497–510.

Van Heuven, S., Pierrot, D., Rae, J.W.B., Lewis, E., Wallace, D.W.R., 2011. MATLAB program developed for CO2 system calculations. ORNL/CDIAC-105b 530.

Vigier, N., Rollion-Bard, C., Levenson, Y., Erez, J., 2015. Lithium isotopes in foraminifera shells as a novel proxy for the ocean dissolved inorganic carbon (DIC). C.R. Geosci. 347, 43–51.

Watson, E.B., 2004. A conceptual model for near-surface kinetic controls on the trace- element and stable isotope composition of abiogenic calcite crystals. Geochim. Cosmochim. Acta 68, 1473–1488.

Weldeab, S., Lea, D.W., Schneider, R.R., Andersen, N., 2007. 155,000 years of West African monsoon and ocean thermal evolution. Science 316, 1303–1307.

White, A.F., 1977. Sodium and potassium coprecipitation in aragonite. Geochim. Cosmochim. Acta 41, 613–625.

Wilkinson and Algeo, T.J., 1989. Sedimentary carbonate record of calcium-magnesium cycling. Am. J. Sci. 289, 1158–1194.

Wit, J.C., de Nooijer, L.J., Haig, J., Jorissen, F.J., Thomas, E., Reichart, G.J., 2017. Towards reconstructing ancient seawater Mg/Ca by combining porcelaneous and hyaline foraminiferal Mg/Ca-temperature calibrations. Geochim. Cosmochim. Acta 211, 341–354.

Wit, J.C., De Nooijer, L.J., Wolthers, M., Reichart, G.J., 2013. A novel salinity proxy based on Na incorporation into foraminiferal calcite. Biogeosciences 10, 6375–6387.

Wolthers, M., Nehrke, G., Gustafsson, J.P., Van Cappellen, P., 2012. Calcite growth kinetics: Modeling the effect of solution stoichiometry. Geochim. Cosmochim. Acta 77, 121–134.

York, D., Evensen, N.M., Martínez, M.L., De Basabe Delgado, J., 2004. Unified equations for the slope, intercept, and standard errors of the best straight line. Am. J. Phys. 72, 367–375.

Yu, J., Foster, G.L., Elderfield, H., Broecker, W.S., Clark, E., 2010. An evaluation of benthic foraminiferal B/Ca and $\delta^{11}B$ for deep ocean carbonate ion and pH reconstructions. Earth Planet. Sci. Lett. 293, 114–120.

Zhou, X., Rosenthal, Y., Haynes, L., Si, W., Evans, D., Huang, K.F., Hönisch, B., Erez, J., 2021. Planktic foraminiferal Na/Ca: A potential proxy for seawater calcium concentration. Geochim. Cosmochim. Acta 305, 306–322.

Zweng, M.M., Seidov, D., Boyer, T., Locarnini, M., Garcia, H., Mishonov, A., Baranova, O.K., Weathers, K., Paver, C.R., Smolyar, I., others, 2019. World ocean atlas 2018, volume 2: Salinity.